ELSEVIER

Journal of Marine Systems 29 (2001) 335–363

JOURNAL OF MARINE SYSTEMS

www.elsevier.nl/locate/jmarsys

The use of digital filter initialization to diagnose the mesoscale circulation and vertical motion in the California coastal transition zone

Robert L. Haney *, Robert A. Hale

Department of Meteorology, Naval Postgraduate School, Monterey, CA, 93943-5001 USA

Received 15 October 1999; received in revised form 2 June 2000; accepted 26 June 2000

Abstract

A dynamical method of initializing the primitive equations is tested and used to diagnose the three-dimensional circulation associated with jets and eddies as found in the California coastal transition zone (CTZ). The initialization method, referred to as digital filter initialization (DFI), was recently developed by [Monthly Weather Review 120 (1992) 1019] for use in an intermittent data assimilation system in the atmosphere. The ability of DFI to recover the mesoscale ageostrophic circulation associated with finite amplitude jets and eddies in the ocean is first demonstrated using control data produced by simulations with a primitive equation model. The DFI method is then applied to synoptic hydrographic data collected during several California CTZ surveys in the summer of 1988. The diagnostic results indicate the existence of jets, eddies, and filaments in the CTZ domain with maximum horizontal currents of the order of 0.6 m/s at the surface. Currents associated with such jets and filaments are coherent to a depth of over 500 m. The surface currents associated with a prominent cool filament are generally confluent, and weakly convergent on average, along the 270 km offshore extent of the filament. Meanders in the jet display convergence and downwelling upstream of pressure troughs and divergence and upwelling downstream of the troughs. Maximum vertical velocities at 100 m are of the order of 10 m/day. This result is consistent with independent estimates of subduction rates made from biological studies in this and similar coastal filaments in the CTZ program. Published by Elsevier Science B.V.

Keywords: Digital filter initialization; Mesoscale circulation; Vertical motion; California coastal transition zone

1. Introduction

When a numerical primitive equation ocean model is integrated forward in time from an initial state of rest, or exact geostrophic balance, the simulated currents and mass field undergo pronounced oscillations as part of the geostrophic adjustment process. This adjustment is responsible for spinning up quasi-geostrophic currents and secondary circulations that are an essential part of the locally "balanced" state of the ocean, or slow manifold (Lorenz, 1992). Under certain conditions, this slow manifold can be described quite accurately by quasi-geostrophic (QG) theory. Indeed, the application of QG theory to quasi-synoptic arrays of ocean hydrographic data (e.g., Leach, 1987; Bower, 1991; Pollard and Regier, 1992; Lindstrom and Watts, 1994; Strass, 1994; Pinot et al., 1996; Rudnick, 1996) or to quasi-Lagrangian surface drifter data (Paduan and

* Corresponding author. Fax: +1-831-656-3061.
E-mail address: haneyrl@met.nps.navy.mil (R.L. Haney).

0924-7963/01/$ - see front matter. Published by Elsevier Science B.V.
PII: S0924-7963(01)00023-9

Niiler, 1990; Swenson et al., 1992) has produced realistic estimates of the three-dimensional circulation and dynamics of upper ocean fronts and mesoscale features.

The foregoing notwithstanding, diagnostic methods based on QG theory have well-known theoretical as well as practical limitations. For example, QG theory is generally not valid for flows involving strong nonlinearities, variable stratification or steep topography. Advanced intermediate models, such as the balanced model, semigeostrophic model and iterated geostrophic model (Allen, 1993; Allen and Newberger, 1993), represent potentially attractive extensions to QG theory; however, they have only recently been used as diagnostic tools with ocean observations (Shearman et al., 2000). In addition, the application of such QG or balanced models to in situ ocean data (e.g., Lindstrom and Watts, 1994; Allen and Smeed, 1996; Rudnick, 1996; Shearman et al., 2000) implicitly assumes that the analyzed mass field accurately represents the slow manifold of ocean variability (Lorenz, 1992), i.e., that the hydrographic analysis is free of disturbances (noise) due to internal waves, tides or other fast, unbalanced modes of variability. Observations of the currents, if available, are usually used only to obtain a nondivergent reference velocity for the determination of the absolute geostrophic velocity (Chereskin and Trunnell, 1996; Rudnick, 1996). They are not otherwise generally used to help determine the slow mode.

In the present study, we try to address some of the above theoretical and practical limitations of QG-based diagnostic methods by taking advantage of the natural selection properties of the geostrophic adjustment process inherent in the primitive equations (PEs). To accomplish this, we make use of a PE-based dynamic initialization procedure called digital filter initialization (DFI), which was recently developed by Lynch and Huang (1992) for use in numerical weather prediction (NWP). As shown by Lynch and Huang (1992), hereafter LH 92, the application of a low-pass digital filter to the time series of model variables generated by short-term backward and forward integrations starting from an uninitialized analysis (i.e., the DFI procedure) removes the high frequency initialization noise from the time series and produces dynamically balanced model fields. Such fields, when used as initial conditions, produce little or no noise when integrated forward in time during a model forecast. In LH 92, it was further shown that the DFI method is essentially equivalent to the method of nonlinear normal-mode initialization (Machenhauer, 1977) used in operational NWP. More recently, Huang et al. (1994) showed that the digital filter initialization procedure has a clear advantage over the normal-mode initialization scheme as all dependent variables in the numerical model are initialized.

The DFI method has been shown to eliminate noise from model forecasts in the atmosphere, and earlier versions of the DFI method have been used to study mesoscale features in the Alboran Sea (Viudez et al., 1996) and the California Current (Chumbinho, 1994; Shearman et al., 2000). The purpose of this study is to test and verify the DFI method within the context of a PE ocean model and then to use the method to diagnose the three-dimensional circulation associated with upper ocean jets and eddies observed in the California coastal transition zone, CTZ (Brink and Cowles, 1991).

2. The digital filter initialization method

In LH 92, the DFI method was used to produce dynamically balanced mass and wind fields, which, when used as initial conditions in an atmospheric prediction model, removed spurious oscillations from the forecast fields. In DFI, a digital filter is applied to the time series of model variables generated by short-term forward and backward integrations of a primitive equation model starting from an uninitialized analysis. The method consists of first integrating the model backward adiabatically (no forcing or friction) from the analysis time, say $t = 0$, to the earlier time $t = -T$, and then integrating the model forward adiabatically from the same initial conditions at $t = 0$ to the later time $t = T$. The resulting time series of model variables (of length $2T$) is then low-pass filtered to produce the dynamically balanced state (slow manifold) corresponding to the time $t = 0$. The filter coefficients with a Lanczos window are given by:

$$h_n = \frac{\sin[n\pi/(N+1)]}{n\pi/(N+1)}\left[\frac{\sin(n\omega_c\Delta t)}{n\pi}\right], \qquad (1)$$

for $n = -N, \ldots N$, with $-T \leq t \leq T$ being the filter domain. Here, $T = N\Delta t$ and $\omega_c = \pi/T$ is the filter cutoff frequency [LH 92]. The dynamically balanced state of a model variable f at $t = 0$, denoted $\tilde{f}_0$, is then given by:

$$\tilde{f}_0 = \sum_{n=-N}^{N} h_n f_n. \quad (2)$$

Since Lynch and Huang were interested primarily in the application of DFI to operational numerical weather prediction, they were motivated to find the largest value of ω_c (smallest $N\Delta t$) that would remove spurious oscillations from the model forecast fields. They arrived at a value of ω_c corresponding to a cutoff period, or filter span ($2T$), of 6 h. Here we test a range of filter spans from $2T = 12$ h to $2T = 36$ h. We also test the effect of iterating the DFI procedure by using the resulting balanced state, $\tilde{f}_0$, as the initial condition for a second application of DFI, etc.

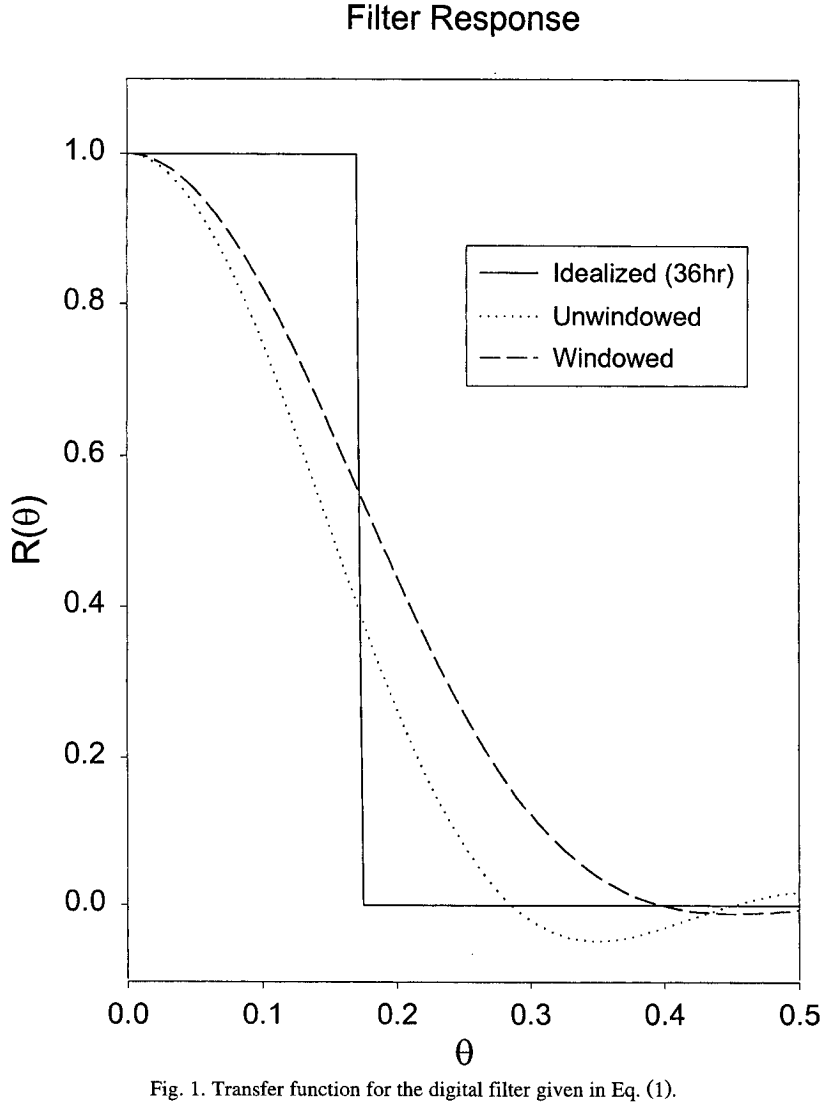

Fig. 1. Transfer function for the digital filter given in Eq. (1).

The transfer function for the windowed filter given in Eq. (1) having a cutoff period of 36 h is shown in Fig. 1. The parameter values are $\Delta t = 1$ h and $N = 36$. The cutoff value of the digital frequency $\theta = \omega\Delta t$ is, therefore, $\theta_c = \pi/18 \sim 0.17$. In this study, we will always use the windowed filter (Eq. (1)), which decreases the Gibbs oscillations for $\theta > \theta_c$ at the cost of widening the pass band beyond the cutoff value [LH 92]. For later reference, it is useful to note that inertial oscillations (period of 19 h at 38°N, Section 4) correspond to a digital frequency of $\theta = 2\pi/19 \sim 0.33$. The transfer function at $\theta = 0.33$ is seen in Fig. 1 to be about 0.07, which means that such inertial oscillations will be largely damped by the DFI procedure using a 36 h cutoff period. In this study, we explore the sensitivity of the DFI solution to the specified cutoff frequency, but not to the form of the filter. We also consider the effect of iterating, or repeating the DFI procedure several times. This effectively lengthens the filter scale and alters the cutoff frequency as well.

3. Testing DFI

In this section, we test the DFI method using control data generated by numerical simulations. The basic objective of DFI as a diagnostic tool is to determine the dynamically balanced three-dimensional circulation from a synoptic, but uninitialized, analysis of the mass and current fields. Because this balance is achieved by geostrophic adjustment, the final state is determined by both the mass and the current analyses, with the initial currents playing a stronger role at the smaller scales and the initial mass field dominating at the larger scales. In this context, the scale separation occurs at the Rossby radius (Gill, 1982, pp. 205–208).

To test the DFI method as a diagnostic tool in the ocean, we first produce a control data set representing a model simulated evolution of a typical oceanic slow mode. At a particular instant during the control simulation, we extract the density field and a reference pressure. These fields, and an approximation to the currents, are then used as initial conditions in the DFI procedure, which is implemented in an attempt to diagnose the actual currents, including the vertical velocity. To examine the effect of the initial currents on the DFI solution, we repeat the initialization procedure using different (approximations to) initial currents. The success of the DFI method is evaluated by comparing the known currents from the control simulation, particularly the vertical velocity, with those from the DFI solution. The control data are from primitive equation model simulations of (a) a meandering jet, (b) a rapidly developing upper-ocean frontal wave, and (c) a circular vortex. All of the test simulations and DFI applications are carried out with the DieCAST ocean model (Dietrich, 1997; Dietrich and Ko, 1994; Dietrich and Lin, 1994), which is a multilevel, rigid lid primitive equation model based on the hydrostatic and Boussinesq approximations. Since the results of the DFI method will depend on a numerical model's ability to simulate geostrophic adjustment, slightly different results may be obtained with different numerical formulations. Such differences are not considered significant at this stage.

3.1. Meandering jet

The control data for the meandering jet was obtained by superposing a small amplitude sinusoidal density disturbance on an otherwise Gaussian meridional density gradient in a 300-km-wide cyclic channel 2 km in depth. The channel was placed on an f plane at 39N, where the inertial period is 19 h. The basic stratification was that of the California Current region and the vertical structure of the density disturbance was that of the first empirical mode in that region (Haney et al., 1995). A disturbance wavelength of 270 km, much larger than the first internal Rossby radius of deformation (21 km), was chosen for this first test. In evaluating DFI as a diagnostic tool, it is important that the mass and current fields in the control simulation are well balanced, i.e., that they represent a true slow mode. This was ensured by starting the control simulation from initial fields produced by a single DFI application with a filter span of 24 h. The initial currents for the DFI procedure were computed from the geostrophic thermal wind equation with the reference level (zero currents) at the bottom (2 km).

After initialization, the model was integrated forward for 18 days, which allowed the large scale disturbance to evolve and propagate. Since the disturbance amplitude was very small, with a Rossby number $R_o \sim 10^{-3}$, the expected evolution is simply that of a quasi-linear first baroclinic mode Rossby wave with the "beta" effect being provided by the weak northward (cross-channel) gradient of mean relative vorticity. The vertical velocities at the depth of the main thermocline at day 18 (Fig. 2a) are very small with maximum values of only 0.02 m/day. As expected for this scale of disturbance, the vertical velocity is essentially that predicted by quasi-geostrophic theory with sinking motion ahead of the pressure ridges and rising motion ahead of the pressure troughs. The maximum vertical velocities occur at the depth of the pycnocline ($\sim$ 500 m) and there is a small downstream tilt as predicted by theory (Pedlosky, 1964).

The DFI solution (Fig. 2b) recovers this slow mode extremely well. A single application of DFI with a total filter span of $2T = 36$ h, or two iterations of DFI with $2T = 24$ h, perform equally well. Using the vertical velocity, W, to quantify the evaluation, we compute the normalized root mean square error $E(z)$ given by:

$$E(z) = \left[\frac{\sum (W_c - W_{DFI})^2}{\sum (W_c)^2} \right]^{1/2}, \qquad (3)$$

where the subscripts c and DFI refer to control and DFI, respectively, and the summation is over the interior of the channel (excluding several rows of grid points near the channel walls) at the depth z. Fig. 3a,b shows $E(z)$ for filter spans of both 24 and 36 h. With $2T = 24$ h, the DFI solution approaches the control ($E \leq 0.1$) only after several iterations. This is because the inertial gravity waves that accomplish geostrophic adjustment have relatively low frequency ($\omega \sim f$) when, as in the present case, the scales are much larger than the Rossby radius. They have relatively higher frequencies ($\omega \geq f$) only when the scales are comparable to or smaller than the Rossby radius (e.g., Gill, 1982, p. 197). Thus, a filter span of 24 h is somewhat too short to complete the geostrophic adjustment of this large scale disturbance, and it is also too short to successfully filter out inertial motion from the time series. With a total filter span of 36 h, which is almost twice the local inertial period, a single application of the DFI procedure is sufficient to produce an accurate solution. We conclude from this result that for scales of motion that are large compared to the internal Rossby radius, a rather long period of integration and filtering, approximately twice the local inertial period, is needed. When this is done, the DFI procedure is generally able to diagnose the control vertical velocities with maximum normalized errors $E(z) \sim 0.1$ (Fig. 3b).

3.2. Frontal wave

The control simulation of an upper-ocean frontal wave is designed to test DFI in a mesoscale situation in which the scales of variability are comparable to the internal Rossby radius and the Rossby number is no longer small. The case chosen is that of a mixed layer front observed in the North Atlantic subtropical convergence zone during the Frontal Air–Sea Interaction Experiment (FASINEX) (Eriksen et al., 1991). The observed frontal evolution was recently shown by Samelson and Chapman (1995), hereafter SC 95, to be due to nongeostrophic baroclinic instability. Thus, it is a strong test of DFI in a physical situation in which quasi-geostrophic dynamics is only marginally valid.

As in the meandering jet simulation described above, the primitive equation model is set up in a cyclic zonal channel, this time 150 km wide and 300 m deep. The length of the channel is 70 km, which corresponds to the wavelength of the most unstable linear mode (Samelson, 1993). The basic state along-channel jet has the form used by SC 95 in which surfacing isopycnals separate two 50- to 100-m-deep regions of vertically uniform surface layer density, which themselves are isolated from the deeper interior by a pycnocline near 150-m depth (SC 95, Fig. 4). The frontal wave has the densest water to the south and peak westward velocities greater than 0.5 m/s at the surface. The resulting Rossby number is 0.5. As in the previous control simulation, a single application of DFI with a total

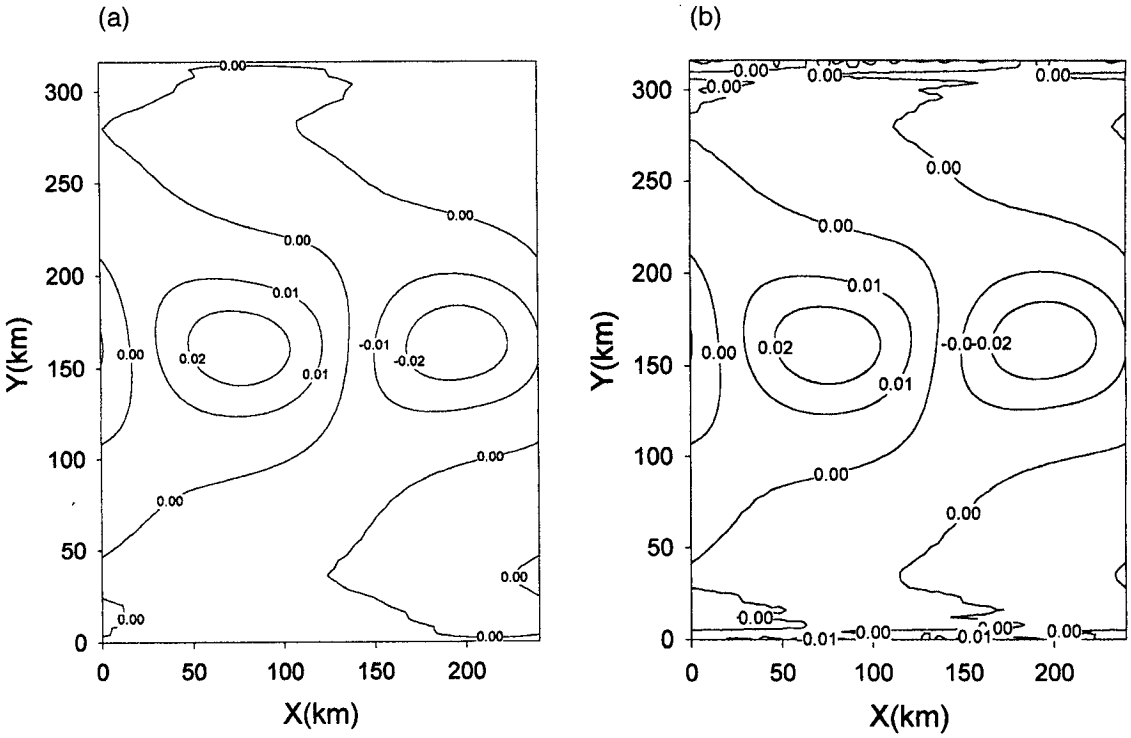

Fig. 2. Vertical velocities (m/day) at 480 m on day 18 from (a) the control simulation of a meandering zonal jet and (b) as diagnosed by DFI.

filter span of 24 h is applied to the initial currents (geostrophic, with reference level at the bottom (300 m)) and density fields in order to help ensure an exclusively slow-mode evolution of the growing front.

The frontal wave grows through baroclinic instability reaching its full amplitude by about day 10. The surface temperature deviations at day 6 of the development show a closed cyclonic eddy just beginning to form (Fig. 4a). The vertical velocity associated with the developing cyclone is shown in Fig. 4b. As in SC 95, a narrow strip of very intense sinking motion (up to 35 m/day) associated with the surface frontogenesis forms upstream (east) of the trough. The compensating rising motion downstream (west) of the trough is weaker and broader. As discussed in SC 95, this strong asymmetry in the pattern of vertical velocity is associated with the surface frontogenesis and it weakens at depths below 50 m (not shown). This kind of asymmetry in the vertical velocity, which was also found by Wang (1993), Strass (1994) and Pinot et al. (1996) in their studies of unstable upper ocean fronts, is a clear indication of the strength of the nonlinearity since linear solutions do not have such asymmetries (Samelson, 1993).

The ability of the DFI method to diagnose the strong ageostrophic flow and vertical velocity in this frontal wave was tested by again using the density, the reference pressure, and geostrophic currents from the control simulation as initial conditions. The resulting DFI solution for the vertical velocity is shown in Fig. 4c. In this case, the total filter span is 36 h and the DFI procedure was repeated a second time (DFI2), using the results of the first DFI application (DFI1) for initial conditions. The pattern of vertical motion in the DFI solution is very similar to that of the control simulation although the DFI solution has a somewhat broader area of slightly weaker sinking motion than is found in the control. This weakening and broadening of the pattern of vertical velocity is partly due to a time-smoothing of the slow mode by

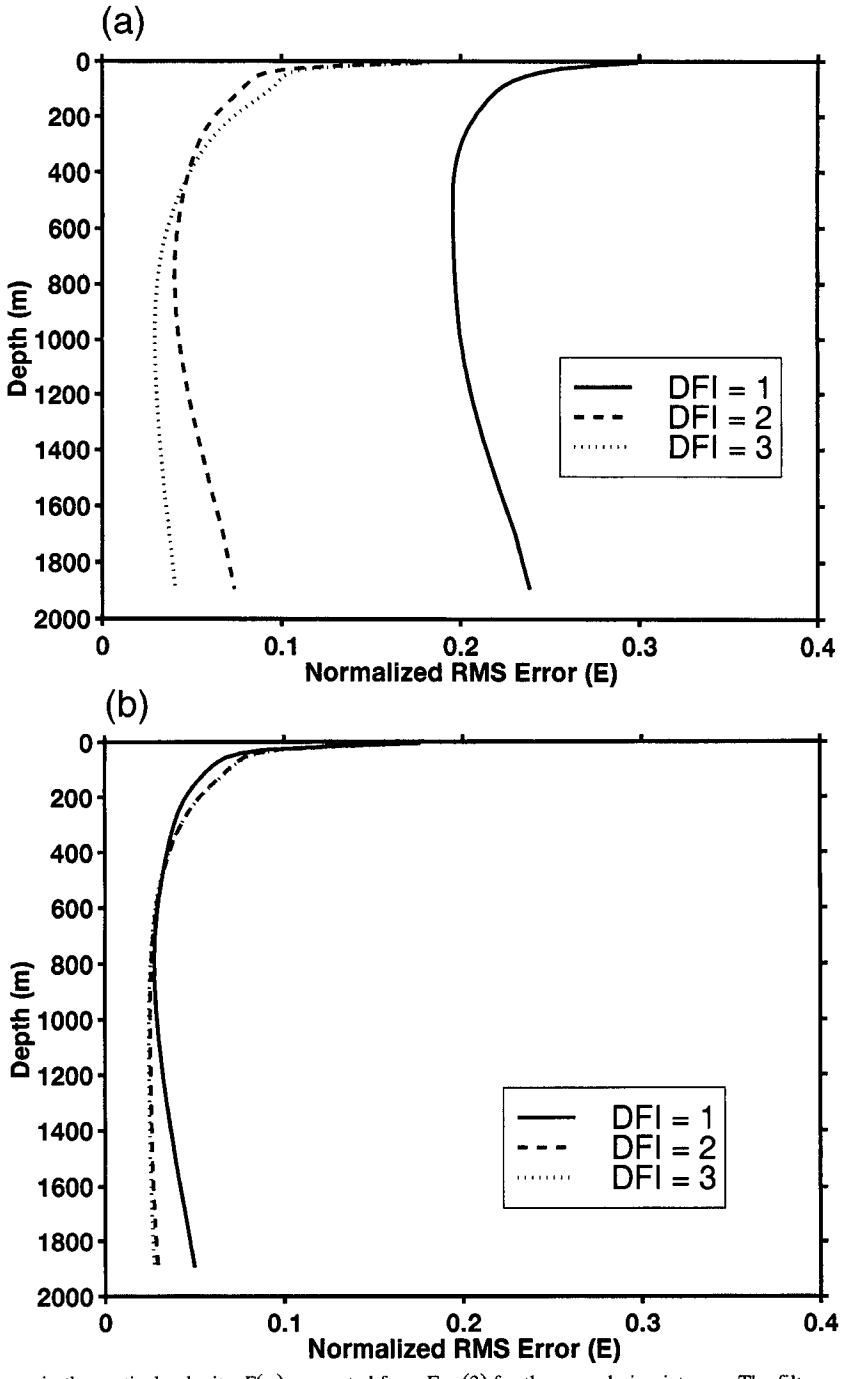

Fig. 3. Normalized errors in the vertical velocity $E(z)$ computed from Eq. (3) for the meandering jet case. The filter span ($2T$) is 24 h in (a) and 36 h in (b).

DFI. In this case, the rapidly developing and propagating frontal wave has a time scale that is short enough that the growing wave itself is somewhat affected (damped) by the DFI filter. Nevertheless,

the pattern and magnitude of the solution for W is quite good and it certainly captures a very large part of the asymmetry in the field caused by the nonlinear development of the wave.

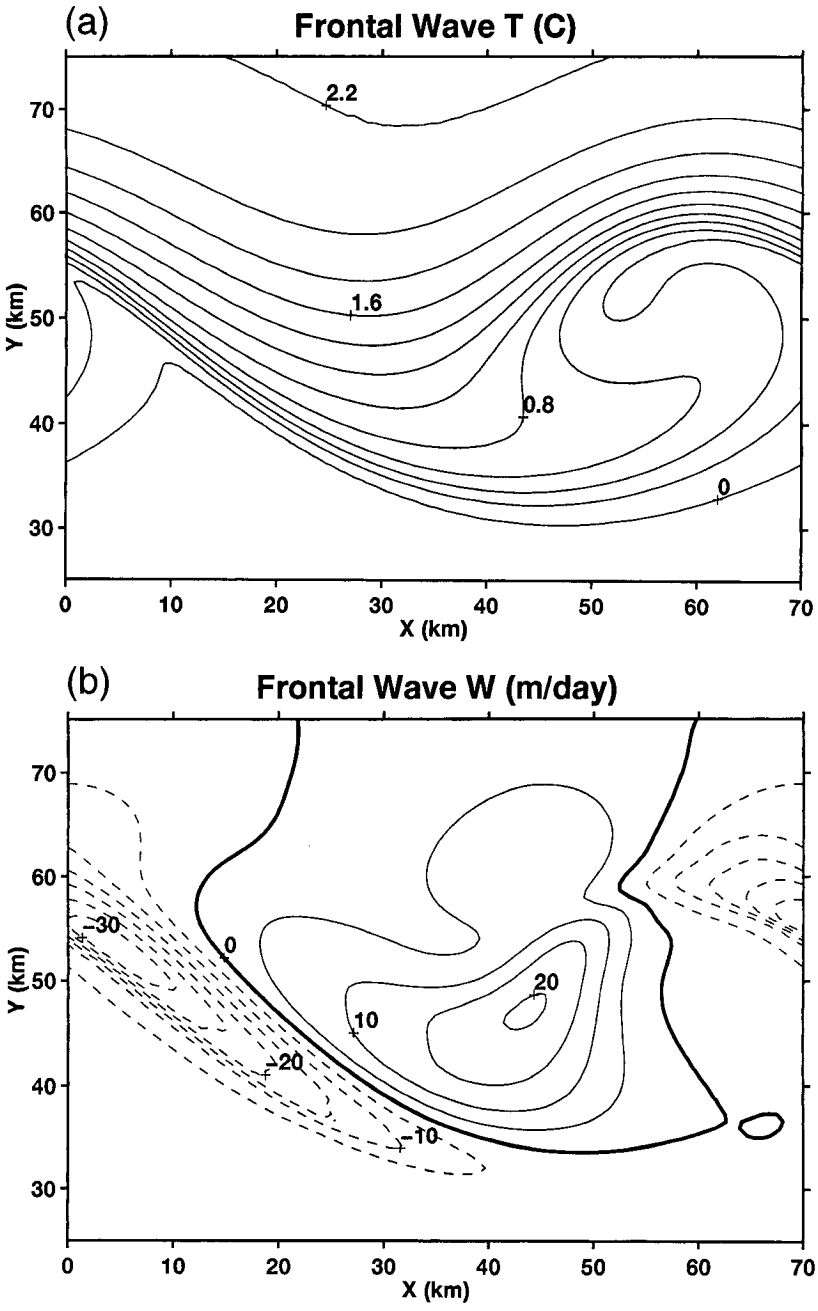

Fig. 4. (a) Temperature deviations (C) at day 6 from the control simulation of a growing baroclinic frontal wave. The contour interval is 0.2°C, with the higher values to the north. Vertical velocity (m/day) at 35 m in the frontal wave on day 6 of the control simulation (b) and as diagnosed by DFI2 (two iterations) using a filter span of 36 h (c). The contour interval for W is 5 m/day, with negative values (sinking motion) dashed.

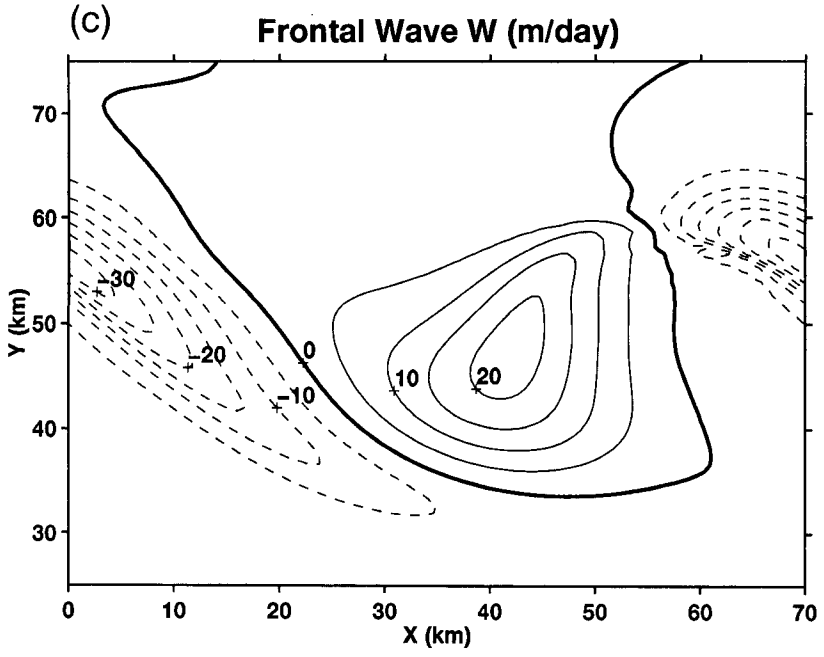

Fig. 4 (*continued*).

Fig. 5 shows the profiles of normalized errors $E(z)$ for the solution in Fig. 4c. It is clear that the second DFI iteration improves the overall solution. It also can be seen that the normalized errors tend to be

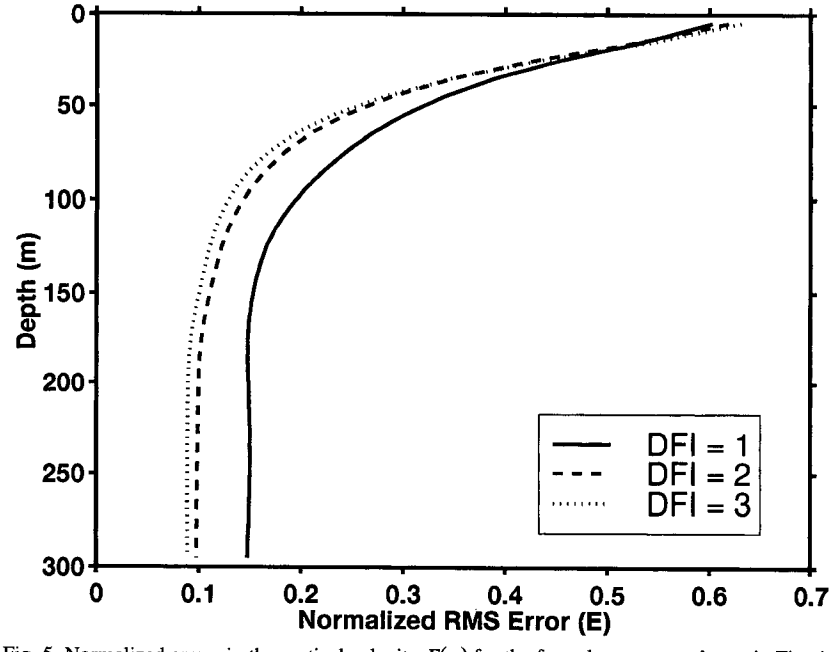

Fig. 5. Normalized errors in the vertical velocity $E(z)$ for the frontal wave case shown in Fig. 4c.

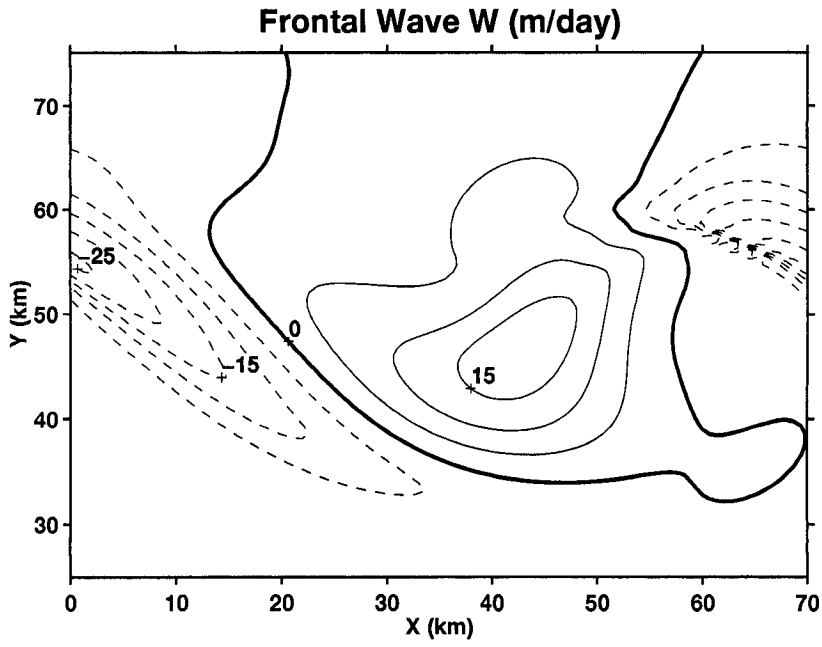

Fig. 6. Vertical velocity (m/day) at 35 m in the frontal wave as diagnosed by DFI1 (one iteration) using a filter span of 36 h and initial currents given by Eq. (4a,b). The contour interval is 5 m/day, with negative values (sinking motion) dashed.

largest near the surface. As noted above, this is because the propagation and development of the wave in the upper ocean, having a time scale of the order of a day or two, is sufficiently fast that the

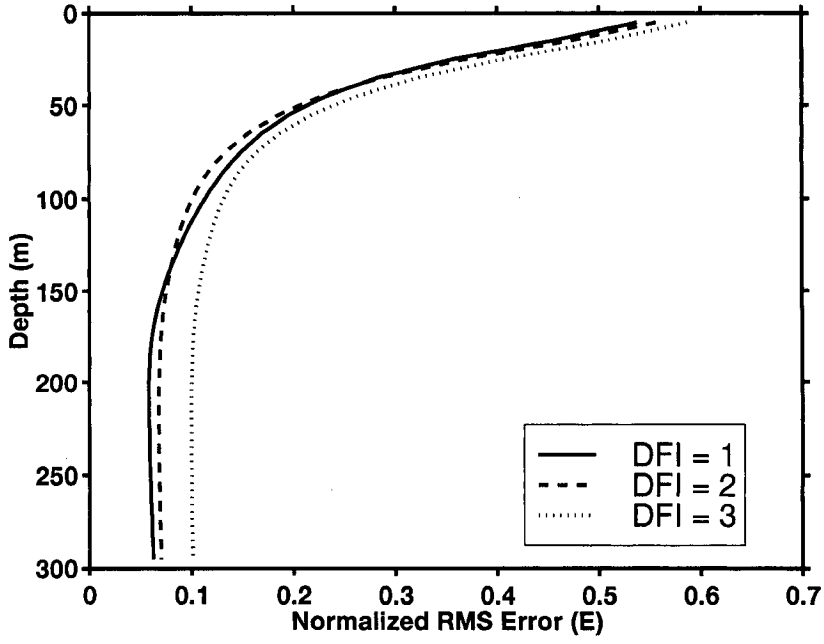

Fig. 7. Normalized errors in the vertical velocity $E(z)$ for the frontal wave case shown in Fig. 6.

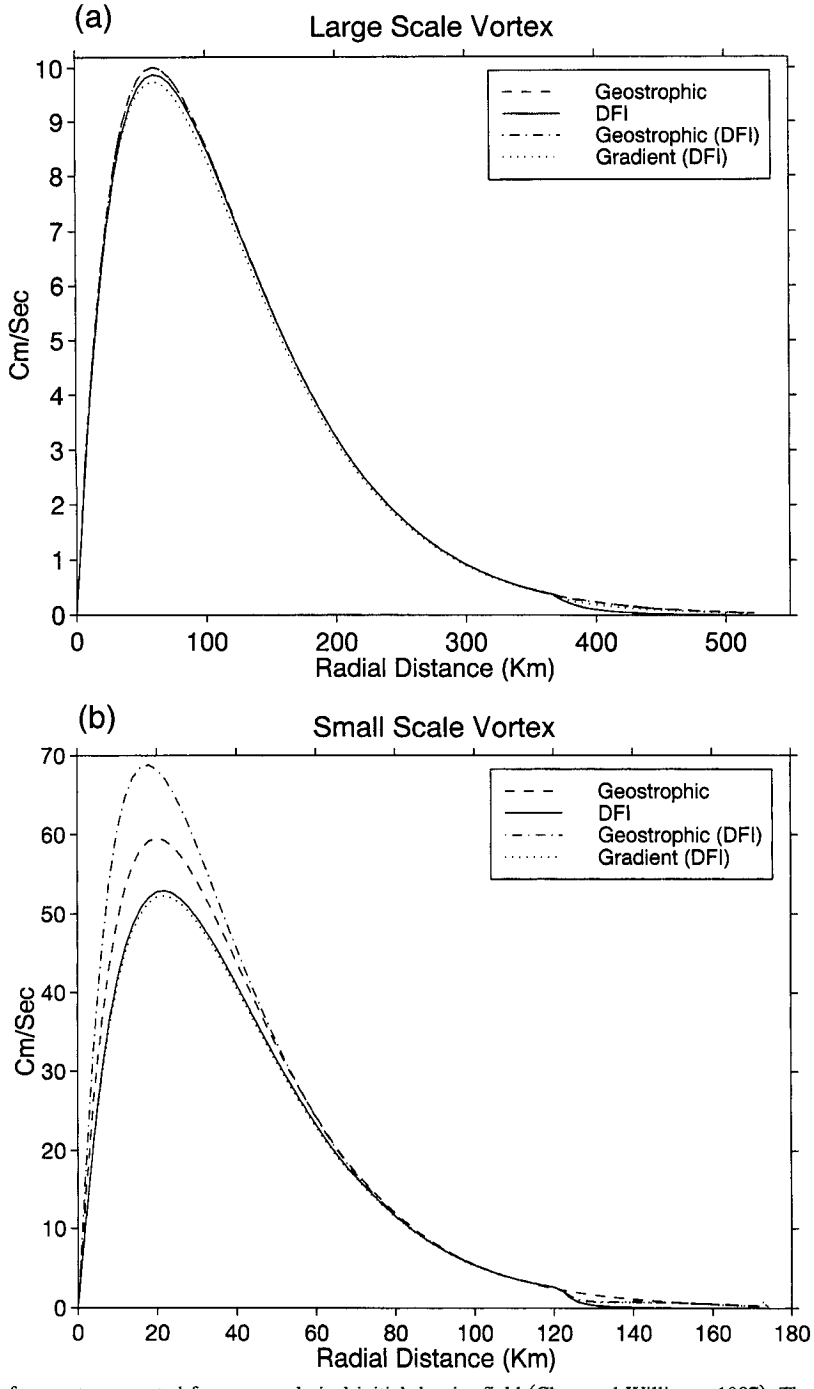

Fig. 8. Radial profile of currents computed from an analytical initial density field (Chan and Williams, 1987). The current profiles shown are: geostrophic currents based on the DFI pressure field (dashed curve), DFI solution (solid curve), geostrophic currents based on the initial pressure field (dash–dot curve) and gradient currents based on the DFI pressure field (dotted curve). The radius of the maximum current is 60 km in (a) and 20 km in (b). See text for additional details.

wave is partly interpreted by DFI as a "fast" mode (see Fig. 1) and, therefore, partly damped by the DFI filter.

To illustrate the importance of the initial currents in DFI, we applied the method to the same frontal wave case; however, instead of geostrophic balance, we used the rotational part of the currents from the control simulation for the initial currents. These were computed at each depth as:

$$(u,v) = \left(-\frac{\partial \psi}{\partial y}, \frac{\partial \psi}{\partial x} \right), \tag{4a}$$

where ψ is the solution to:

$$\nabla^2 \psi = \zeta_c \tag{4b}$$

subject to $\psi = p_c/(\rho_0 f)$ on the boundaries. Here ζ_c and p_c are the vorticity and pressure, respectively, from the control simulation. The difference between the currents given by Eqs. (4a,b) and those given by geostrophic balance is that Eqs. (4a,b) includes the rotational part of the ageostrophic currents present in the control simulation. This test, therefore, evaluates the impact on the diagnosed vertical velocity of using a more accurate representation of the initial currents. Whether it is possible, in practice, to observe ocean currents to such a degree of accuracy, i.e., including the rotational part of the ageostrophic flow, is an entirely separate issue that is not addressed here.

Fig. 6 shows the DFI solution for the vertical velocity, and Fig. 7 shows the error profile $E(z)$ for this test. It can be seen that the vertical velocity associated with the growing frontal wave is recovered better than before, and that the errors in the upper ocean, which are associated with the relatively small scale of the frontal wave, are also reduced. At 35 m, for example, where the vertical velocity is close to its maximum, the normalized error is less than 0.3. Furthermore, this improved solution is obtained with only one DFI iteration. The diagnostic results are improved because the rotational part of the control currents given by Eqs. (4a,b) is a more accurate representation of the actual currents than is geostrophy. This is especially true on the relatively small scale of the frontal wave. On these smaller scales, the initial currents play a more important role

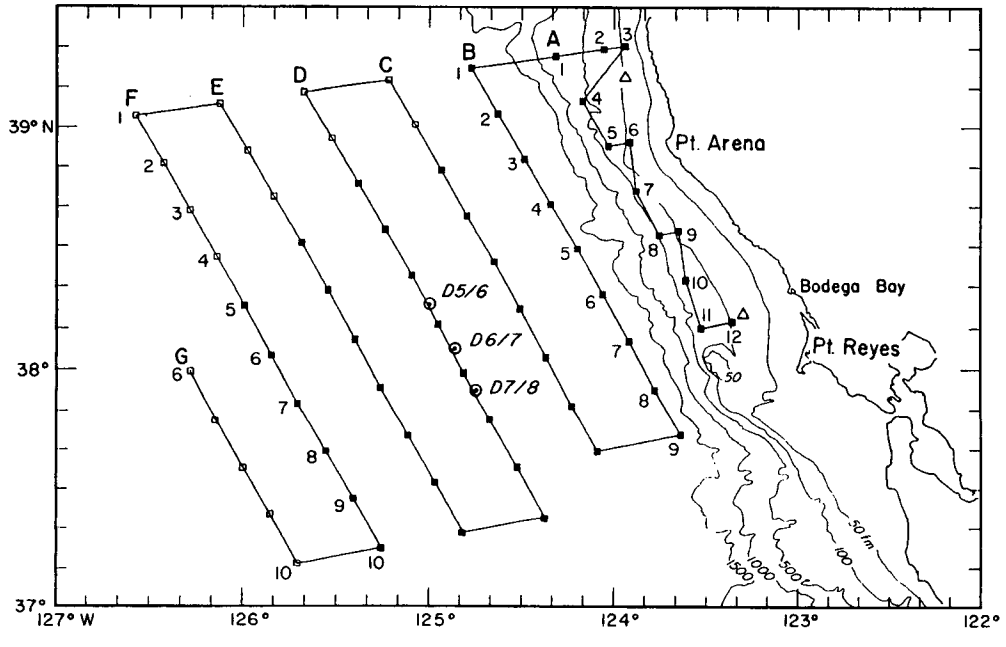

Fig. 9. The standard station grid for repeated surveys of the coastal transition zone off northern California, June–August 1988. Letters designate alongshore sections, and numbers designate station positions along each section. Triangles represent NDBC meteorological buoys and circles represent current meter moorings. From Huyer et al. (1991).

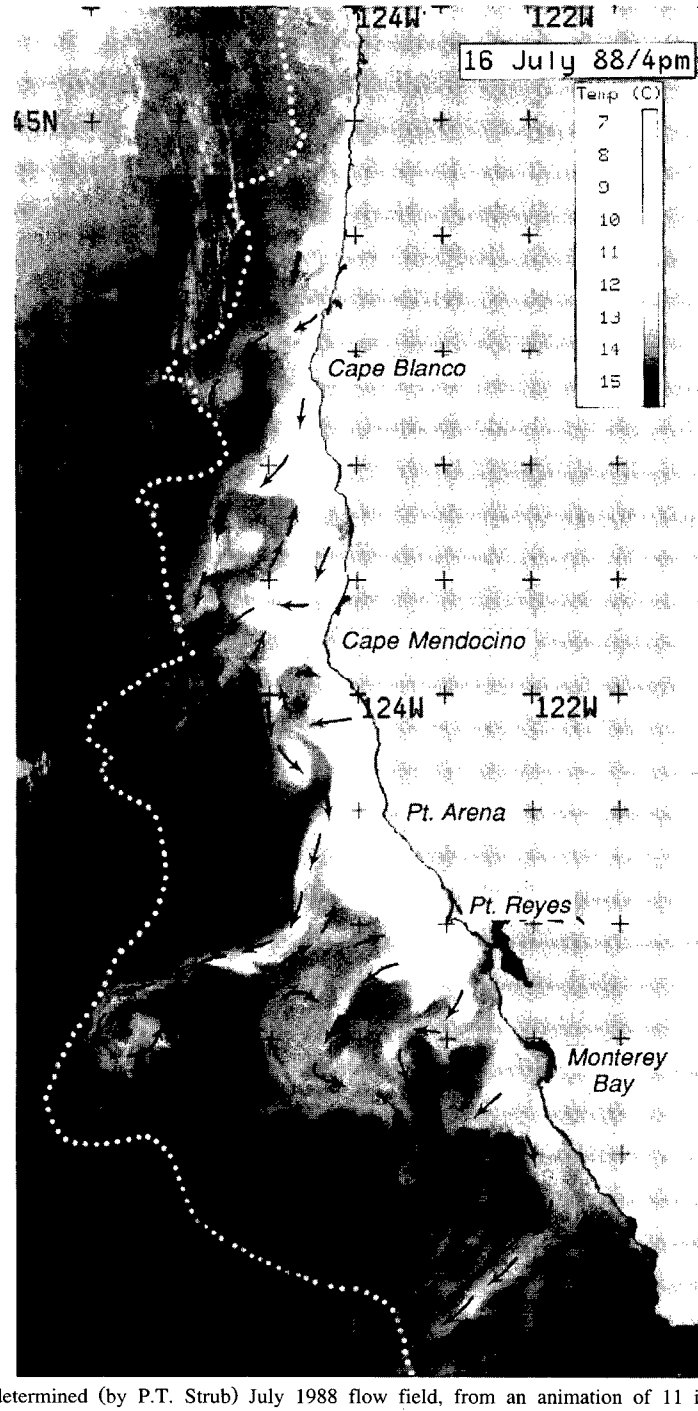

Fig. 10. The subjectively determined (by P.T. Strub) July 1988 flow field, from an animation of 11 images on July 16–18, 1988, superimposed on the satellite SST field from July 16. The black arrows depict the direction of the flow, not the magnitude of the velocities. The white dotted line traces the path taken by a surface drifter in September–October 1984 (Thomson and Papadakis, 1987). Although the drifter was from a different year and month than the July 1988 satellite images, it traces out a path similar to the outer edge of the region of cold filaments in the July images. From Strub et al. (1991).

in determining the balanced state through the geostrophic adjustment mechanism. Improving the initial currents, therefore, improves the diagnosed vertical velocities. This result demonstrates how important it is to have a good analysis of the initial currents, including if possible the rotational part of the ageostrophic currents as in Eqs. (4a,b), in order to diagnose the smaller (frontal) scales. Using more accurate initial currents cannot, however, remedy a fundamental limitation of DFI, which is that its balanced state (slow manifold) is constrained by the filter cutoff period, which in this case is 36 h. Since the upper-ocean frontal evolution is relatively "fast," i.e., it occurs on a time scale that is not much greater than 36 h, it is definitely affected (damped) by the filter. This fundamental limitation of DFI is the reason for the larger errors in the upper ocean part of the error profile in Fig. 7.

3.3. Circular vortex

As noted above, ocean variability that has a time scale that is comparable to or less than the cutoff period of the filter used in DFI is significantly damped by the filter (Fig. 1). Such variability, if it is part of the "slow mode," cannot be accurately diagnosed by DFI. This is somewhat unfortunate because in many realistic ocean situations where the Rossby number is not small, and one would like to use a higher order diagnostic method like DFI, the time scales are relatively short. This was the situation in the frontal wave case where the time scale of the wave near the surface, i.e., the advective time scale, was of the order of a few days. To test the DFI in a more optimal setting, where the Rossby number is not small yet the time scale of the slow mode is large compared to the cutoff period, we consider a station-

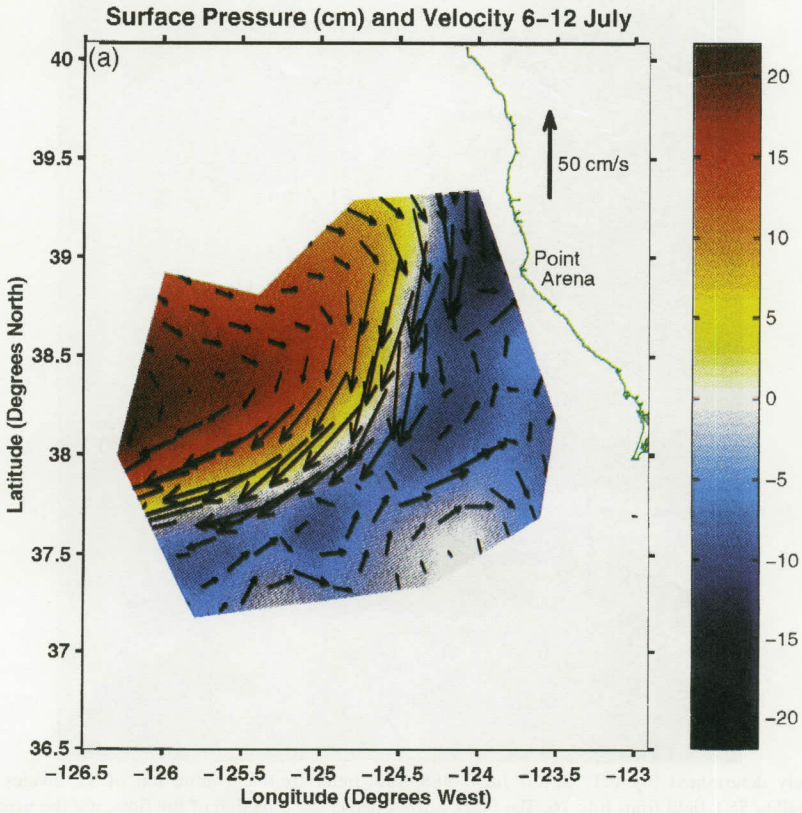

Fig. 11. Maps of the surface pressure field (scaled by $\rho_0 g$, color bar in cm) and current vectors (arrows with scale on the right) diagnosed by DFI for the CTZ surveys during (a) July 6–12, (b) July 13–18, and (c) July 22–26, 1988. The full domain (36.5N to 40.2N and seaward to 126.5W) was used in DFI, but results are shown only in the region sampled by the particular survey.

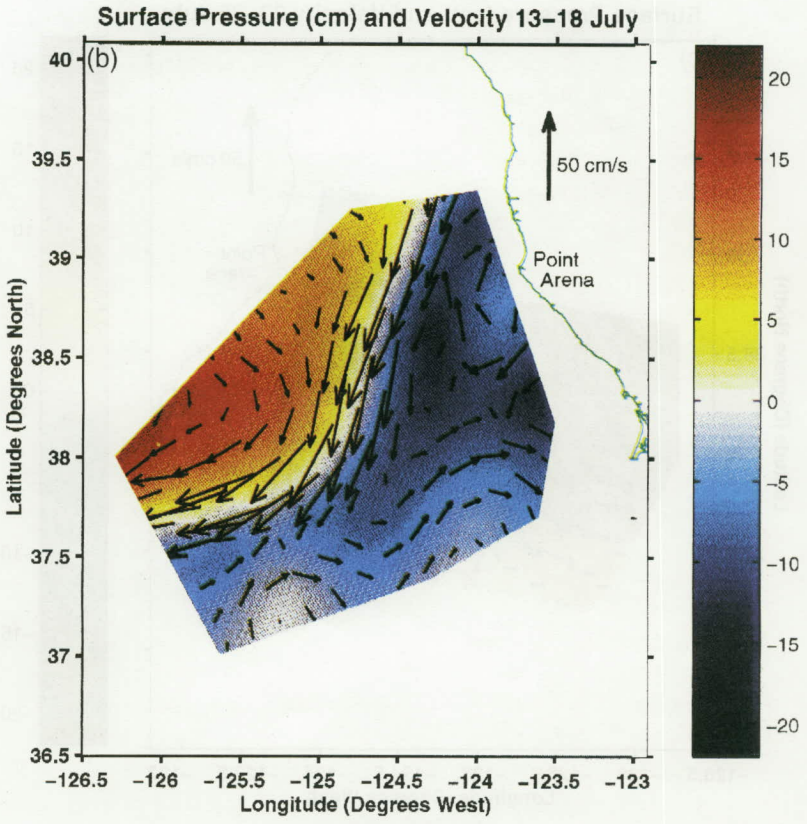

Fig. 11 (*continued*).

ary circular vortex of the type studied by Chan and Williams (1987). For this test we define a radially symmetric analytic disturbance density field with an idealized vertical structure superposed upon a horizontally uniform stratification typical of the region (Haney et al., 1995). The domain depth was 1 km, giving a basic Rossby radius of 20 km (see below). Although the fields are three-dimensional, for simplicity, we only show the currents at the surface as a function of the distance from the center of the vortex. As before, the initial currents were computed from the geostrophic thermal wind equation with the reference level at the bottom (1 km).

Fig. 8 shows the results of applying DFI to both a large scale vortex (a) and a small scale vortex (b). For the large scale vortex, the basic stratification was decreased by a factor of four and for the small scale vortex it was increased by a factor of 4. The altered stratification resulted in a Rossby radius of 10 km for the large scale vortex and 40 km for the small scale vortex, thus making the small scale vortex even smaller in the dynamical sense. The large scale vortex, with peak velocities of only 10 cm/s at 60 km from the center, is essentially geostrophic, with almost no curvature effects. Since the scale of the vortex (60 km) is much larger than the Rossby radius (10 km), there is also little or no adjustment of the density field during the DFI.

The small scale vortex on the other hand, with peak velocities over 50 cm/s at 20 km from the center (Fig. 8b), is quite different. Near the radius of maximum currents, the Rossby number, $V/(fR)$ with R the radius of curvature, is about 0.3. Thus, the acceleration due to flow curvature is not insignificant. Since the vortex is steady, the slow-mode solution is known to be that of gradient balance (e.g., Holton, 1992, p. 67). The results presented in Fig. 8b show that the DFI solution, starting from geostrophic

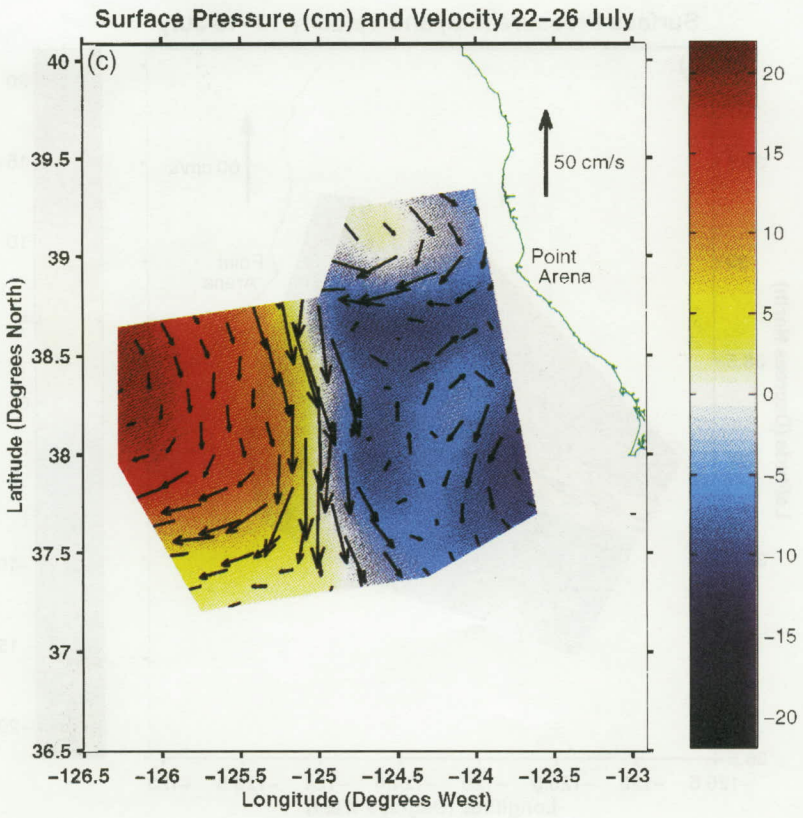

Fig. 11 (*continued*).

initial conditions, has diagnosed this type of balance quite well. The DFI balanced currents (solid curve) are essentially the same as the gradient currents computed from the DFI balanced pressure field (dotted curve). Because the vortex is cyclonic, the DFI balanced currents are subgeostrophic. That is, they are weaker than the geostrophic currents computed from the DFI balanced pressure field (dashed–dot curve). Since the horizontal scale of the vortex (20 km) is somewhat smaller than the Rossby radius (40 km), both the density and the currents have been altered from their initial values by the DFI process. The currents have decreased from an initial (geostrophic) peak value of almost 60 cm/s (dashed curve) to the final (DFI) peak value of 53 cm/s. At the same time, the vortex pressure gradient, which is directly proportional to the geostrophic current, has increased. The geostrophic currents computed from the DFI solution (dash–dotted curve) are larger than the initial geostrophic currents (dashed curve). This intensification of the vortex pressure gradient by the DFI process is a direct result of using geostrophic currents, which are stronger than the corresponding gradient currents, as initial conditions. Since the mass field on these smaller scales tends to adjust toward the currents during geostrophic adjustment, the vortex pressure gradient is increased.

The result of this test simply demonstrates the ability of DFI to diagnose the balanced ageostrophic currents accurately in the case when the balanced state is evolving sufficiently slowly. The test also illustrates the important role of the initial currents in determining the DFI solution when the scales of motion are comparable to the Rossby radius. Thus, to diagnose the true slow mode in such a case in practice, one must have an accurate estimate of the slow-mode currents at the initial time. Although other tests of DFI as a diagnostic tool may also be

useful, e.g., the effect of observational noise on the diagnosed slow mode, the remainder of this paper is devoted to an application of the method to the California Current.

4. Application of DFI to the coastal transition zone off northern California

The coastal transition zone off northern California, which refers to the region seaward of the continental shelf, is heavily populated with eddies, jets and filaments commonly found in other eastern boundary current regions, especially during the upwelling season. In the late 1980s, the coastal transition zone (CTZ) program was carried out to investigate the structure, dynamics and biological implications of these coastal features (Brink and Cowles, 1991). As part of this program, five successive surveys of a mesoscale sampling grid (Fig. 9) were completed between mid-June and early August 1988 (Huyer et al., 1991). The major feature observed during each survey was a cold filament extending southwestward offshore from Point Arena (Fig. 10). The filament remained nearly stationary during the first 4 weeks of the CTZ program; however, its position and orientation changed considerably within a period of just a few days in mid-July. Associated with the filament was a baroclinic equatorward jet with core velocities greater than 0.5 m/s at the surface. Observational evidence from upper ocean profiles of radon (Kadko et al., 1991), as well as from anomalous T–S properties of deep, high chlorophyll containing layers along the axis of the filament (Washburn et al., 1991), indicate that subduction of near surface isopycnal layers may occur at

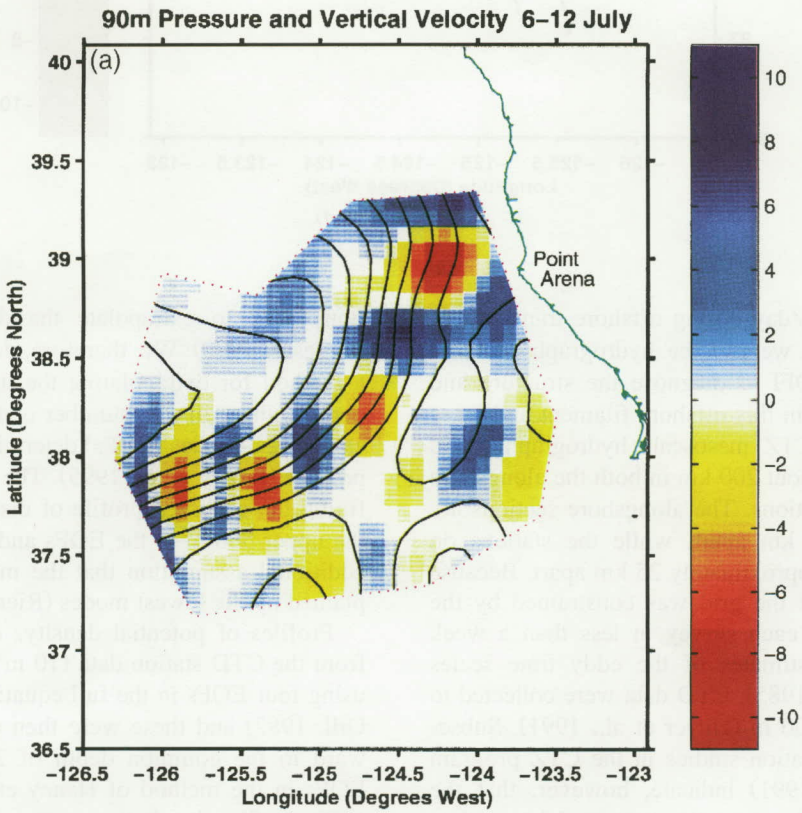

Fig. 12. Maps of the pressure field scaled by $\rho_o g$ (isolines with contour interval of 4 cm) and vertical velocity (color bar in m/day) at 90-m depth diagnosed by DFI for the CTZ surveys during (a) July 6–12, (b) July 13–18, and (c) July 22–26, 1988. Results are shown only in the region sampled by the survey.

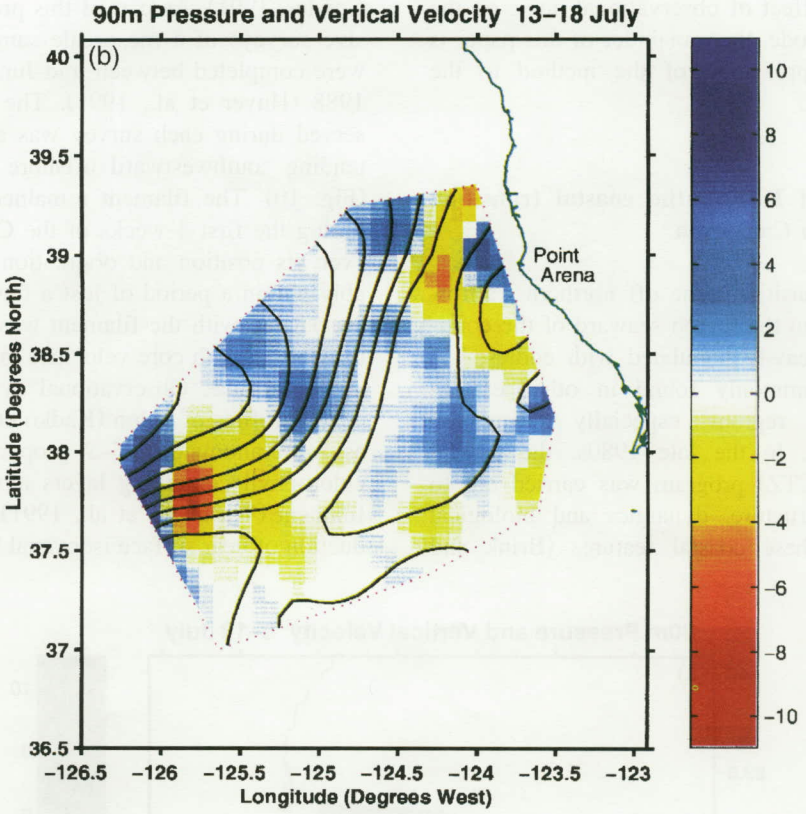

Fig. 12 (*continued*).

rates of 10–15 m/day during offshore transport. In the present study, we use the hydrographic survey data along with DFI to diagnose the structure and vertical velocities in this offshore filament and jet.

The standard CTZ mesoscale hydrographic grid (Fig. 9) extends about 200 km in both the alongshore and offshore directions. The alongshore sections are approximately 40 km apart, while the stations on each section are approximately 25 km apart. Because the overall size of the grid was constrained by the need to complete each survey in less than a week based on prior estimates of the eddy time scales (Rienecker et al., 1985), CTD data were collected to a depth of only 500 m (Huyer et al., 1991). Subsequent data assimilation studies in the CTZ program (Walstad et al., 1991) indicate, however, that the observed disturbances actually penetrated deeper than 500 m, and our early diagnostic studies with this data indicated that the results were sensitive to assumptions used to extrapolate the data below 500 m (DeJesus, 1990). We, therefore, developed and tested a method for extrapolating the upper ocean data to depth using a limited number of full column empirical vertical modes (EOFs) determined from historical profiles (Haney et al., 1995). The method consists of fitting the observed profile of disturbance density in the upper 500 m to the EOFs and making use of the additional assumption that the most variance is explained by the lowest modes (Rienecker et al., 1987).

Profiles of potential density, σ_θ, were computed from the CTD station data (10 m vertical resolution) using four EOFs in the full equation of state (IES80; Gill, 1982) and these were then extrapolated downward to the common depth of 2000 m using four EOFs in the method of Haney et al. (1995). A few CTD profiles in shallow water (< 500 m) on the shelf were available from each survey; however, these were not used in this study because topo-

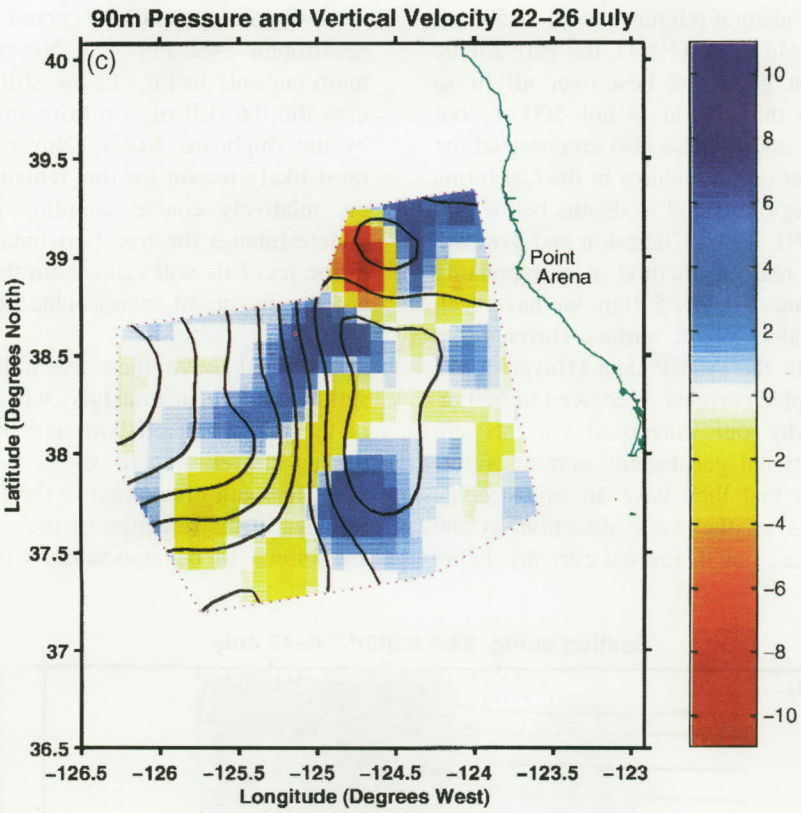

Fig. 12 (*continued*).

graphic effects, as well as possible effects of the irregular coastline, were neglected. The now complete (common depth) profiles of σ_θ were then interpolated to a $(1/12)^\circ$ latitude–longitude grid with 20 levels in the vertical (6 levels are placed in the upper 100 m and 15 are in the upper 700 m). This was accomplished using the method of multi-quadric biharmonic (MQB) interpolation (Nuss and Titley, 1994). The MQB method is a "global" interpolation scheme, which does not introduce artificial scales in data void areas and it does not introduce scales smaller than the spacing between data points. These are important considerations because the observational grid spacing was of the order of the first internal Rossby radius (25 km) and we wanted to resolve that scale with reasonable accuracy in the model. Since the model domain used in the DFI integrations is somewhat larger than the region of ocean observations (see Fig. 11), the ability of the MQB method to extend the analysis benignly into these data void areas is important. The resulting σ_θ analysis, along with geostrophic currents with a reference level of 690 m (Walstad et al., 1991), was used to provide initial conditions for the DieCAST model, which was integrated both forward and backward adiabatically in the DFI procedure, which was executed with a 36 h filter span. The diagnostic results, which we consider to be representative of the balanced circulation at the time of each survey, are presented in Figs. 11–16.

The dominant feature in all three surveys is a strong, approximately geostrophic, jet directed offshore toward the southwest as seen in the satellite picture (Fig. 10) and in the DFI diagnosed surface pressure and current fields (Fig. 11). The maximum surface currents in the core of the jet are a little more than 0.6 m/s. The diagnosed currents are about 20% stronger than those computed geostrophically by

Huyer et al. (1991) using a reference level of 500 m. As shown by Walstad et al. (1991), the geostrophic reference level that gives the best over all fit to ADCP currents in this region is not 500 m, but 600–700 m. Other studies have also emphasized the fact that many upper ocean features in the California coastal transition region extend to depths below 500 m (Ramp et al., 1991, 1997; Chereskin and Trunnel, 1996). By using a realistic method of extrapolating the density disturbances below 500 m, we have been able to diagnose values of the surface currents that compare better with the ADCP data (Huyer et al., 1991) than geostrophic currents referenced to 500 m. Another reason why our diagnosed currents are stronger than traditional geostrophic currents referenced to 500 m is that they have an ageostrophic contribution that is in the same direction as the geostrophic flow, i.e., our diagnosed currents, being generally anticyclonically curved, are slightly supergeostrophic (see Fig. 15). Nevertheless, the maximum currents in Fig. 11 are still somewhat weaker than the 0.6–1.0 m/s maximum currents measured by the shipboard ADCP (Huyer et al., 1991). The most likely reason for this remaining discrepancy is the relatively coarse sampling grid, which likely underestimates the true horizontal pressure gradient in the jet. This will cause both the geostrophic flow and the diagnosed ageostrophic flow to be underestimated.

As noted above, there was a dramatic shift in the surface pattern in mid-July, when the northern part of the jet moved offshore and the southern part of the jet moved toward shore, establishing a more north-to-south orientation to the jet (Fig. 11c). Such changes in the direction of the jet, or jet meanders, are known to be associated with areas of vertical

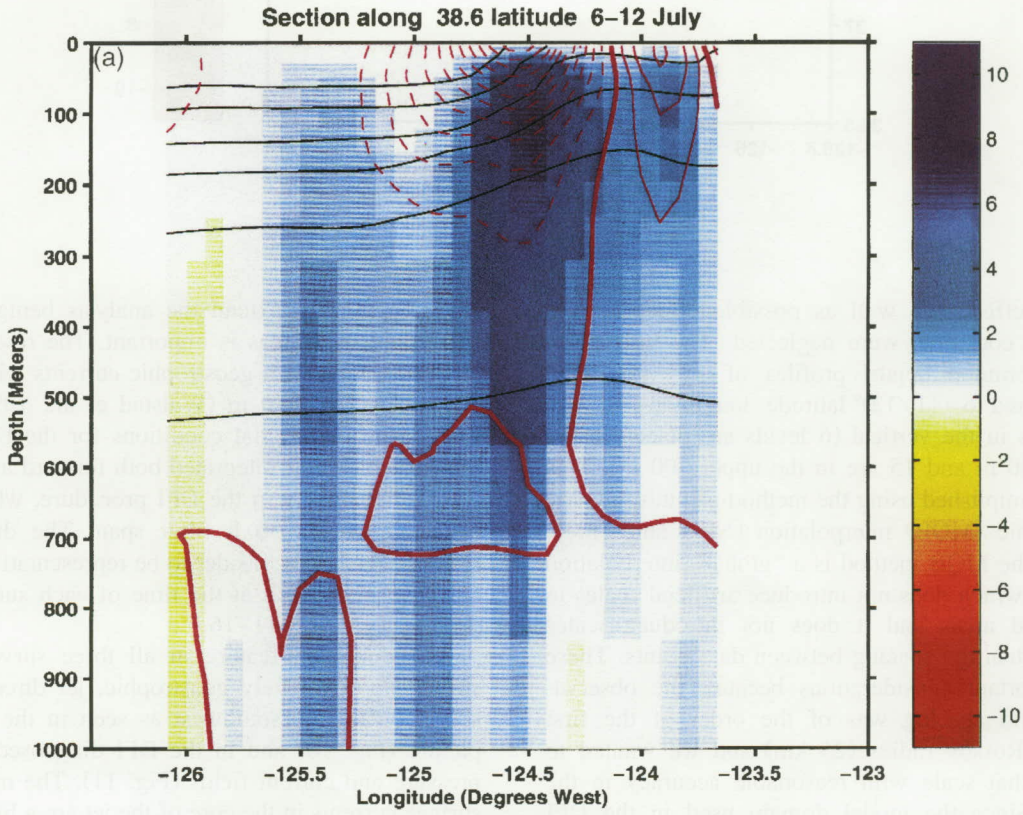

Fig. 13. Vertical sections of potential density, σ_θ (black curves with contour interval of 0.2 kg/m^3), across-section velocity component (magenta curves with contour interval of 5 cm/s), and vertical velocity (color bar in m/day). The sections are from the July 6–12 survey and are (a) zonal along 38.6N and (b) meridional along 125.3W.

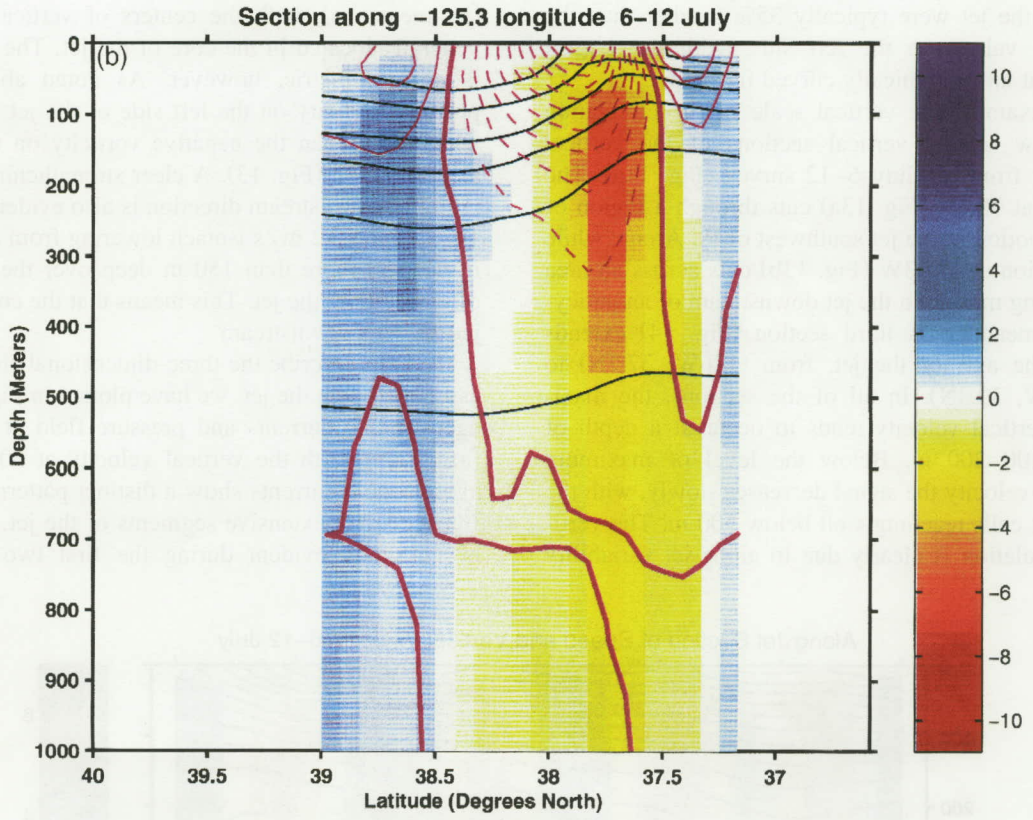

Fig. 13 (*continued*).

motion (Bower and Rossby, 1989). Meanders in an otherwise straight jet produce along-stream variations in relative vorticity, which lead to generally large downstream advections of vorticity and, therefore, to large forcing of quasi-geostrophic vertical velocity (Hoskins et al., 1978; Tintore et al., 1991; Lindstrom and Watts, 1994; Allen and Smeed, 1996; Rudnick, 1996). This is clearly true in the case of the present jet as can be seen in Fig. 12. During the three CTZ surveys the diagnosed vertical velocities are generally as large as ± 10 m/day, with the extreme values occurring in regions of especially strong flow and sharp curvature. For example, on the first mesoscale survey (July 6–12, Fig. 12a) there is an area of sinking motion ($W \sim -10$ m/day) approximately 40 km west of Pt. Arena where the alongshore equatorward jet north of Pt. Arena meanders slightly seaward. This region is then followed approximately 40 km downstream by a region of equally strong rising motion where the jet meanders cyclonically back toward the coast. The high sensitivity of the diagnosed vertical velocity to relatively small, almost imperceptible, meanders in the jet is clearly seen in the analysis, which shows alternating regions of rising and sinking motion associated with such small meanders all along the axis of the jet. Two regions of especially strong vertical velocity also occur off Pt. Arena on July 22–28 (Fig. 12c) in connection with the sharp (cyclonic) curvature of the jet mentioned earlier.

To quantify the significance of the jet meanders, we computed the relative vorticity (ζ) scaled by f for each of the three surveys (not shown). The positive values of ζ/f on the left side of the main jet (facing downstream) range from 0.2 to 0.35 at the sea surface and from 0.1 to 0.15 at 90-m depth. Maximum values occur at cyclonically curved meanders in the jet. Negative values of ζ/f on the right

side of the jet were typically 35% smaller than the positive values on the left side, with the largest values at anticyclonically curved meanders.

To examine the vertical scale of the circulation we show several vertical sections of the vertical velocity from the July 6–12 survey (Fig. 11a). The section at 38.6N (Fig. 13a) cuts through a region of rising motion in the jet southwest of Pt. Arena, while the section at 125.3W (Fig. 13b) cuts across an area of sinking motion in the jet downstream of an anticyclonic meander. A third section (Fig. 14) extends along the axis of the jet, from (126W, 37.7N) to (124.4W, 39.3N). In all of the sections, the maximum vertical velocity tends to occur at a depth of about 100–200 m. Below the level of maximum vertical velocity the signal decreases slowly, with the stronger cells reaching well below 500 m. The vertical circulation is clearly due to along-jet variability (jet meanders), with the centers of vertical motion generally located in the core of the jet. The jet itself is not symmetric, however. As noted above, the positive vorticity on the left side of the jet is somewhat larger than the negative vorticity on the right side of the jet (Fig. 13). A clear strengthening of the jet in the downstream direction is also evident in Fig. 14, with the 0.2 m/s isotach lowering from about 80 m deep to more than 150 m deep over the 270-km distance along the jet. This means that the core of the jet deepens downstream.

To help describe the three-dimensional circulation associated with the jet, we have plotted in Fig. 15 the ageostrophic currents and pressure field at the surface, along with the vertical velocity at 90 m. The ageostrophic currents show a distinct pattern of confluence along extensive segments of the jet, and this is especially evident during the first two surveys

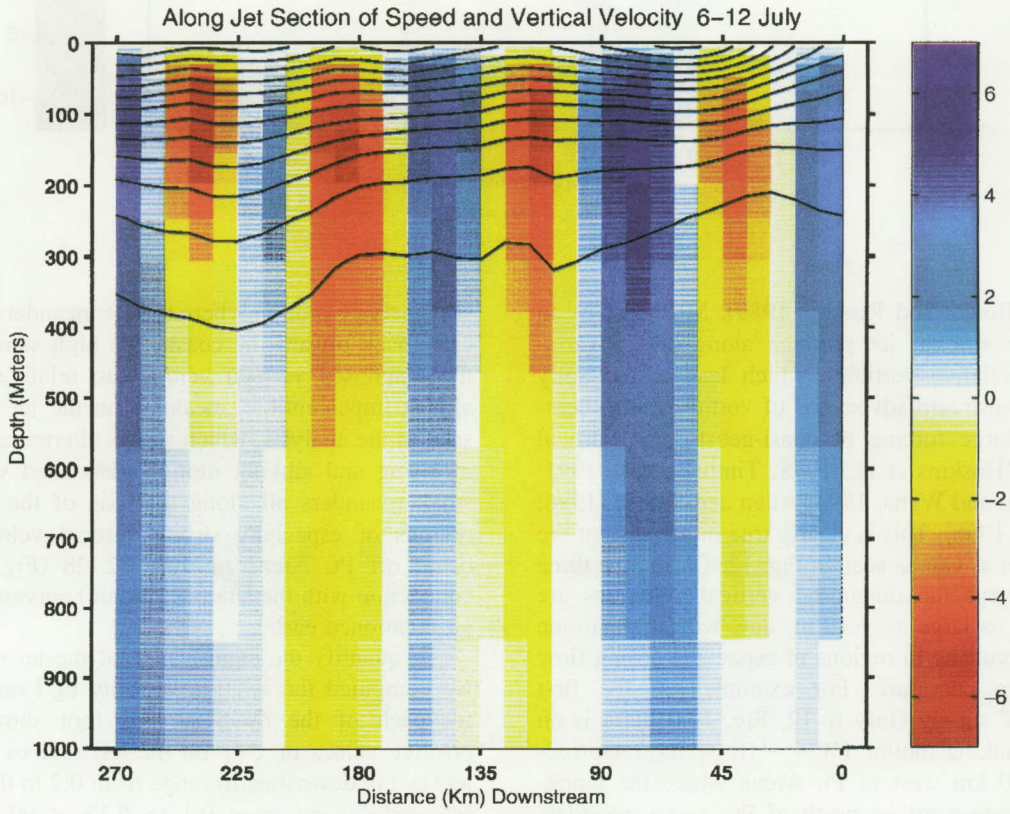

Fig. 14. Along-jet section of current speed (black curves with contour interval of 5 cm/s), and vertical velocity (color bar in m/day). The section is from the July 6–12 survey and follows the core of the jet at the surface which is approximately along the zero isoline of pressure (white color) in Fig. 11.

(Fig. 15a, b). The surface geostrophic flow is also confluent along the jet as indicated by the decreased spacing of the isobars in the downstream direction (Fig. 15). The motion of surface drifters analyzed by Brink et al. (1991) and Swenson et al. (1992) also revealed a clear pattern of confluence into this jet. Such confluence helps to maintain, or perhaps intensify, the across-jet density gradient at the surface, i.e., the surface front. It does not by itself imply horizontal convergence and sinking along the jet because the along-stream flow is diffluent (increasing in the downstream direction) as shown in Fig. 14.

To examine the issue of convergence and confluence more directly, we show in Fig. 16 the along-jet mean vertical and horizontal velocities as a function of depth from the DFI results during the first CTZ survey. The average speed in the jet is about 0.55 m/s at the surface, decreasing to zero near 700-m depth (the reference level). The along-jet mean vertical motion is negative, with a maximum of -0.4 m/day at a depth of about 110 m. This implies mean convergence above 110 m and divergence below 110 m. However, the mean sinking motion of 0.4 m/day is clearly much less than the vertical velocities induced by the jet meanders, which are up to ± 10 m/day (Fig. 12). The jet is, therefore, both confluent and convergent in the upper 100 m on average, but the along-jet variations (meanders) clearly dominate the local circulation.

As a general rule, the ageostrophic flow in the core of the jet is in the same direction as the jet itself, especially in the western two-thirds of the domain where the curvature of the jet is anticyclonic. That is, the anticyclonically curved jet is slightly supergeostrophic. This is to be expected in gradient

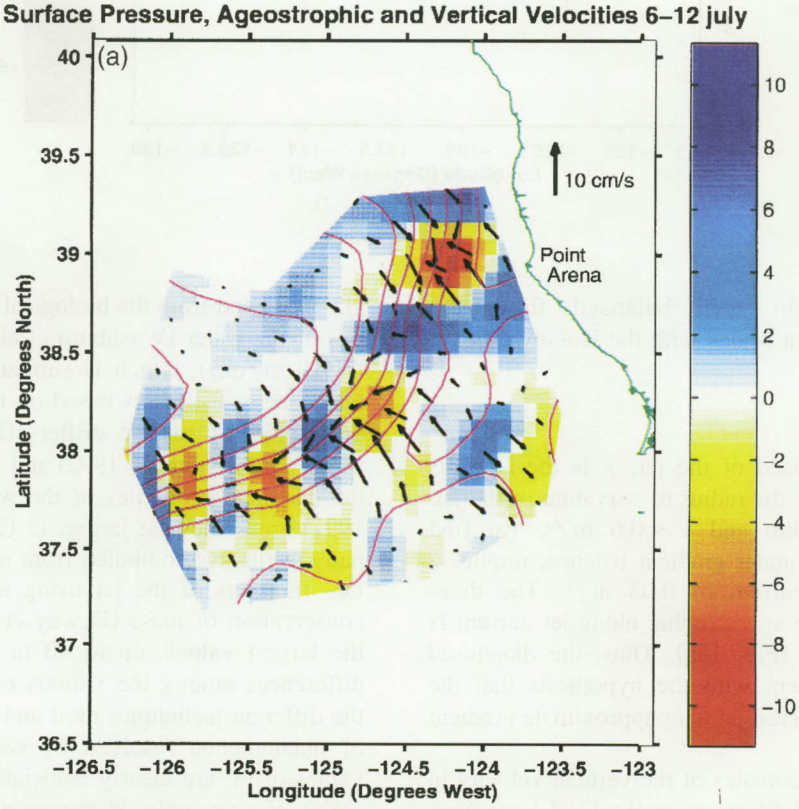

Fig. 15. Maps of the surface pressure field scaled by $\rho_0 g$ (magenta isolines with contour interval of 4 cm), the ageostrophic velocity at the surface (arrows with scale on the right) and the vertical velocity at 90 m (color bar in m/day). The results are for the CTZ surveys during (a) July 6–12, (b) July 13–18, and (c) July 22–26, 1988.

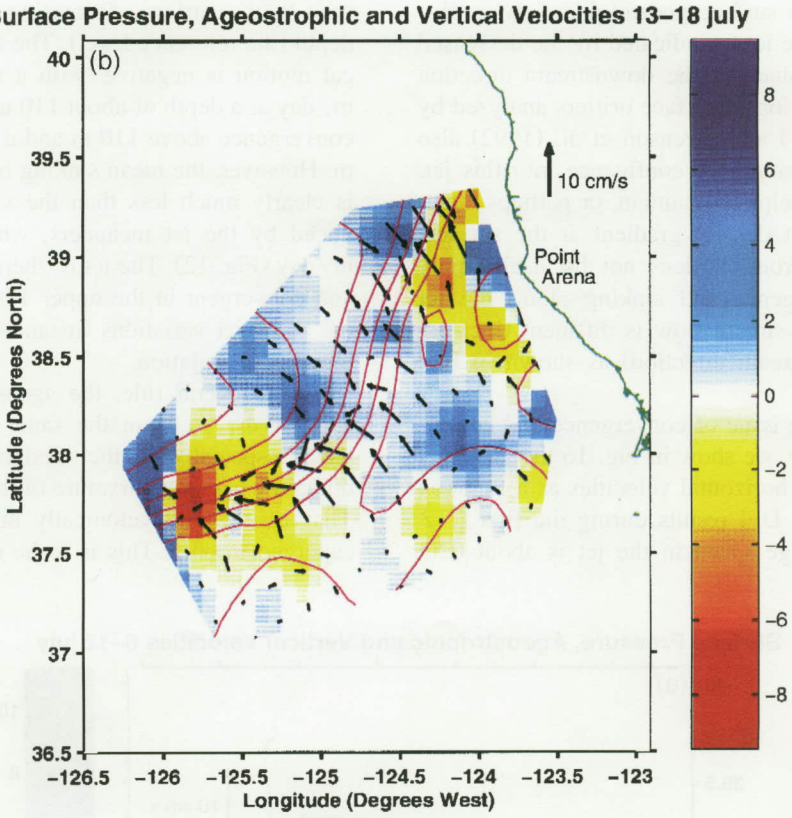

Fig. 15 (*continued*).

balanced flow. In such balanced flow, the ageostrophic current scales with the Rossby number given by:

$$R_o = V/(fR),$$

where V is the speed of the jet, f is the Coriolis parameter and R is the radius of curvature of the jet. Taking $R \sim 130$ km and $V \sim 0.6$ m/s, we find $R_o \sim 0.05$, which, under gradient balance, implies a supergeostrophic current of 0.03 m/s. The diagnosed value of the ageostrophic along-jet current is also of this order (Fig. 15a). Thus, the diagnosed results are consistent with the hypothesis that the anticyclonically curved jet is in approximate gradient balance.

Observational estimates of the vertical velocity in this and other cold filaments in the CTZ have been made by a variety of methods. Estimates of W from the average convergence of surface drifters (Brink et al., 1991) and from the biological and optical properties of the water (Washburn et al.,1991) give values O (10 m/day), which is similar to the results obtained here. Estimates based on the vorticity budget of clusters of surface drifters (Paduan and Niiler, 1990; Swenson et al., 1992) and from an analysis of the chemical properties of the water (Kadko et al., 1991) are somewhat larger, O (20–25 m/day). Finally, estimates computed from repeated microstructure transects of the jet using an equation for the conservation of mass (Dewey et al., 1991) produce the largest values, up to 40 m/day. Much of the differences among the various estimates are due to the different techniques used and the different scales of phenomenon resolved by each method. Larger values of W are clearly associated with the smaller scales. For example, Shearman et al. (2000) studied the vertical velocity in a similar, but somewhat shallower, meandering equatorward jet using higher

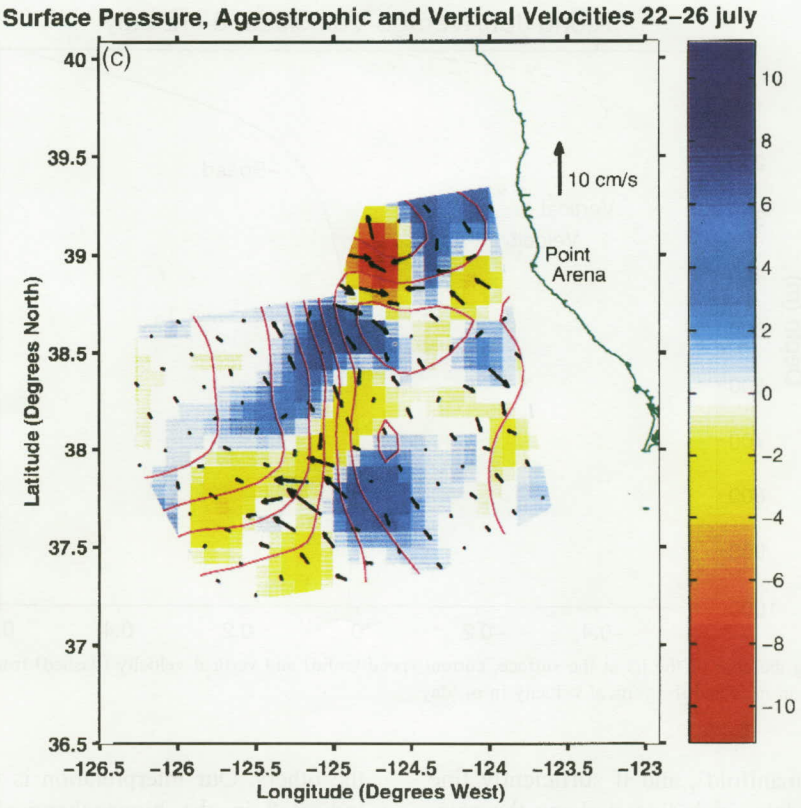

Fig. 15 (*continued*).

order diagnostic methods including the DFI technique used here. They obtained vertical velocities O (30 m/day) primarily because the very high resolution SeaSoar survey ($\Delta x \sim 2$ km, $\Delta y \sim 10$ km) was able to resolve the small scale structure and meanders in the jet. We, therefore, suspect that our estimate of the vertical velocity in the present filament would be increased if the surveys had been able to resolve such smaller scales.

We have also attempted to compare quantitatively our diagnosed vertical velocities with those obtained by other CTZ investigators using different methods. In doing so, we find a clear correspondence and agreement during the first survey between our alternating pattern of vertical velocities along the jet (Fig. 12a) and the values obtained by Swenson et al. (1992) in the same region (their Figs. 7 and 9). This close correspondence is simply a reassuring result, however, since Swenson et al. computed the vertical velocity from the vorticity budget of a cluster of drifting buoys that were caught in the jet during the time of the first survey. The similar results simply confirm the fact that along-jet variability, or jet meanders, are associated with significant vorticity advections and vertical motions. Dewey et al. (1991) computed the mean vertical velocities from repeated high resolution transects along the CTZ line "D" (Fig. 9) during the 2-week period July 2–16, 1988. The resulting vertical sections of vertical velocity (their Figs. 14 and 16) show features with very short vertical scales, representing large vertical shears (fronts). Across the middle of the jet, for example, Dewey et al. show vertical velocities of O (40 m/day) with opposite signs separated in the vertical by less than 50 m. Our study does not capture such strong vertical velocities and short vertical scales, perhaps because of insufficient across-jet resolution in the CTZ survey data. The tests in Section 3 indicate that the DFI method would be able to diagnose such vertical velocities, if in fact they are

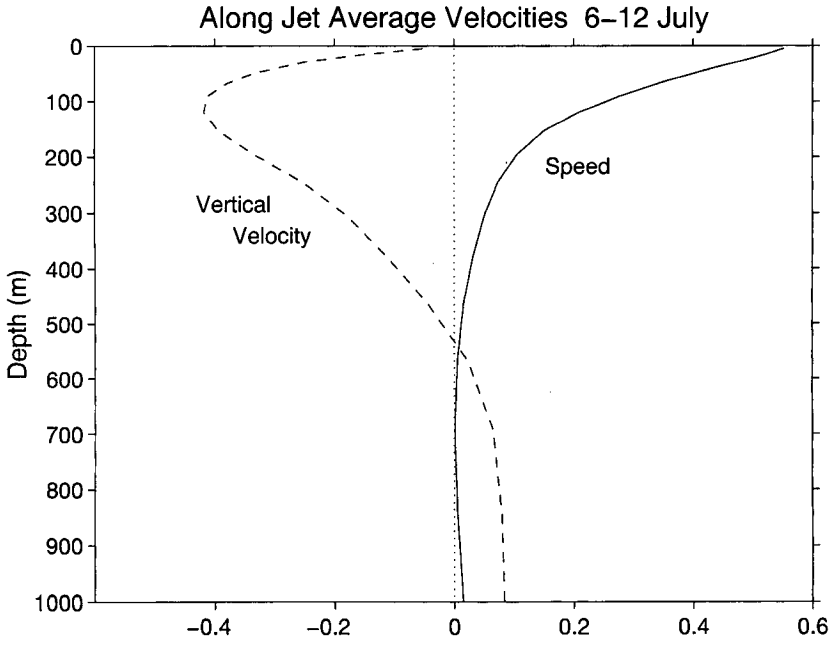

Fig. 16. Average, along the core of the jet at the surface, current speed (solid) and vertical velocity (dashed) from Fig. 14. The abscissa gives the current speed in m/s and the vertical velocity in m/day.

part of the 'slow manifold', and if sufficiently fine resolution survey data, including perhaps the rotational part of the ageostrophic currents, were available. The difference between our pattern of vertical velocities and those of Dewey et al. (1991) is important dynamically. Our symmetric pattern of alternating cells of rising and sinking motion along the core of the jet is typical of a meandering jet. On the other hand, the pattern in Dewey et al. shows not only stronger vertical velocities, but also a distinct across-jet asymmetry, with rising motion on the warm side and sinking motion on the cold side. This implies a direct vertical and across-jet circulation characteristic of a quasi-steady strongly confluent jet, or an unstable baroclinic wave. Diagnostic studies using higher resolution survey data would seem to be required to shed further light on this issue.

Comparing our vertical velocities with the regions of subduction in Washburn et al. (1991) was inconclusive. In the three CTZ surveys, Washburn et al. identified subduction at 21 locations that were well inside the survey data region. Of those 21 points, we diagnosed sinking motion at 7 of them, rising motion at 4 of them and essentially zero vertical velocity at the others. Our interpretation is that the subduction indicated in the biogeochemical measurements of Washburn et al. is too patchy in space to be compared with what is essentially a quasi-geostrophic diagnostic result from synoptic hydrographic survey data.

5. Summary and conclusions

In this study, we have successfully tested and used the method of digital filter initialization (DFI) as a diagnostic tool for ocean analysis. The DFI method consists of applying a digital filter to the time series of primitive equation model variables generated by short-term backward and forward integrations starting from an uninitialized analysis. To test DFI as a diagnostic tool, we used control data generated by idealized simulations using a primitive equation model. In these tests, we generally used the control density field and geostrophic currents as initial conditions. One or two iterations of the DFI method with a filter span of 24–36 h was shown to produce fields of vertical velocities with normalized

rms errors less than 0.1 in the case of a large scale meandering baroclinic jet, and less than 0.3 in an intense, and rapidly evolving, upper ocean front. Use of geostrophic currents, instead of the rotational part of the control currents, at the initial time, degrades the results somewhat in the upper-ocean frontal case. This particular test demonstrated the value of having accurate current measurements in diagnostic studies of ocean phenomenon that have spatial scales comparable to the Rossby radius. In flows with significant depth averaged currents, knowledge of the true reference-level pressure field as used in these tests, in addition to the density field, is needed to obtain the above results.

A fundamental limitation of DFI is its requirement that the balanced state, or "slow mode," be sufficiently "slow." That is to say, the time scale of the slow mode should be large compared to the cutoff period, or filter span, $2T$. This cutoff period is not arbitrary, however. It must be large enough to allow the primitive equation model to complete the geostrophic adjustment process. If the slow mode is not sufficiently slow in comparison to the cutoff period the DFI solution will be a somewhat damped (time-filtered) representation of the true slow mode (see Fig. 1). A slight damping of the slow mode was seen in the near surface layers of the frontal wave test because in that case the time scale of the evolving front was not sufficiently long compared to the filter span. When the time scale of the slow mode is indeed sufficiently large, the DFI solution is quite accurate. This was shown in the case of the stationary vortex for which the solution is gradient balance.

An important aspect of DFI which clearly differentiates it from other advanced diagnostic methods, such as the iterated geostrophic (IG) method (Allen, 1993; Shearman et al., 2000) or the balance equations (BE) method (Gent and McWilliams, 1983), is its dependence on the initial analyzed currents. When the scales of motion are comparable to the Rossby radius, geostrophic adjustment operates in such a way that the mass and density fields tend to adjust toward the (initial) currents. Thus, to accurately diagnose such scales using DFI it is important that the initial currents represent as accurately as possible the rotational part of the true slow-mode currents. In practice, this requirement may place a rather severe demand on the observational system; however, it is an essential consideration when using DFI as a diagnostic tool. The IG and BE methods on the other hand assume that the analyzed density field represents that of the slow mode. The analyzed currents are only used in connection with the geostrophic relation to establish the reference level for the pressure gradient (e.g., Rudnick, 1996). Because of the mutual adjustment of mass and currents that occurs during geostrophic adjustment when the scales of motion are comparable to the Rossby radius, the DFI method may offer some advantages over IG when diagnosing such scales in the presence of observational noise. For example, the method may identify and retain those parts of the analyzed fields (currents and density) that are in a slow-mode balance, and at the same time remove, via the dispersive nature of the geostrophic adjustment mechanism, those parts of the analyzed fields (i.e., the "noise") that are not in such a balance. Although this possibility may warrant future study, it is well beyond the scope of the present paper. A discussion and interpretation of the IG, BE, and DFI diagnostic methods applied to observed flows with a large Rossby number can be found in Shearman et al. (2000).

The DFI method was then applied to quasi-synoptic hydrographic data collected during several California CTZ surveys during the summer of 1988. The data were objectively analyzed to model grid points and extended to the deep ocean using the first four empirical modes (EOFs) computed from historical data. The diagnostic results indicate the existence of a prominent filament in the CTZ domain with maximum currents of the order of 0.6 m/s at the surface. This is somewhat stronger than surface geostrophic currents referenced to a realistic level of 700 m, thus demonstrating that the generally anticyclonically curved filament was supergeostrophic. Because of the vertical extrapolation procedure used with the density data, the currents associated with the filament were coherent to a depth of over 500 m. The surface ageostrophic currents were generally confluent, and weakly convergent on average, along the 270 km offshore extent of the filament. We found no evidence for an asymmetric across-jet circulation and vertical velocity that one generally expects in a confluent frontal jet; however, this could simply be due to the relatively coarse sampling of the hydrographic data. The strongest vertical velocities, of

order 10 m/day at 100 m, were associated with meanders in the otherwise straight jet. These meanders produced convergence and downwelling downstream of the pressure ridges, where the coastal jet was generally directed offshore, and divergence and upwelling downstream of pressure troughs, where the jet was generally directed onshore. This type of meander-induced vertical motion is consistent with that expected from the conservation of potential vorticity, and it is similar to that found in Gulf Stream meanders (Bower and Rossby, 1989; Lindstrom and Watts, 1994). The diagnosed pattern of vertical velocity is consistent with independent estimates of subduction in this and similar coastal filaments made from biological studies in the CTZ program; however, the magnitudes diagnosed here are somewhat smaller.

Acknowledgements

We are especially grateful to Tim Stanton for use of the CTZ hydrographic data, to Wendell Nuss and Pom Sirayanone for use of the MBQ analysis method, and to Ted Strub for providing Figs. 9 and 10 used in this study. We are also grateful to our NPS colleagues Terry Williams and Steve Ramp, as well as former students Roland DeJesus and Rogerio Chumbinho, for valuable discussions and input on the topic of this paper. This work was sponsored by the Navy Ocean Model and Prediction (NOMP) program (Code 322OM) of the Office of Naval Research, and the Naval Postgraduate School, whose support is gratefully acknowledged. The manuscript was efficiently prepared by Mrs. Penny Jones.

References

Allen, J.S., 1993. Iterated geostrophic intermediate models. Journal of Physical Oceanography 23, 2447–2461.

Allen, J.S., Newberger, P.A., 1993. On intermediate models for stratified flow. Journal of Physical Oceanography 23, 2462–2486.

Allen, J.T., Smeed, D.A., 1996. Potential vorticity and vertical velocity at the Iceland Faeroes front. Journal of Physical Oceanography 26, 2611–2634.

Bower, A.S., 1991. A simple kinematic mechanism for mixing fluid parcels across a meandering jet. Journal of Physical Oceanography 21, 173–180.

Bower, A.S., Rossby, T., 1989. Evidence of cross-frontal exchange processes in the Gulf Stream based on isopycnal RAFOS float data. Journal of Physical Oceanography 19, 1177–1190.

Brink, K.H., Cowles, T.J., 1991. The coastal transition zone program. Journal of Geophysical Research 96, 14637–14647.

Brink, K.H., Beardsley, R.C., Niiler, P.P., Abbott, M., Huyer, A., Ramp, S., Stanton, T., Stuart, D., 1991. Statistical properties of near-surface flow in the California coastal transition zone. Journal of Geophysical Research 96, 14693–14706.

Chan, J.C.L., Williams, R.T., 1987. Analytical and numerical studies of the beta-effect in tropical cyclone motion: Part I. Zero mean flow. Journal of the Atmospheric Sciences 44, 1257–1265.

Chereskin, T.K., Trunnell, M., 1996. Correlation scales, objective mapping, and absolute geostrophic flow in the California Current. Journal of Geophysical Research 101, 22619–22629.

Chumbinho, R.P.A., 1994. Kinematics and dynamics of a cyclonic eddy off Pt. Arena, California. PhD dissertation, Naval Postgraduate School, 83 pp.

DeJesus, R., 1990. A diagnostic study of the velocity structure of a meandering jet using a primitive equation model with dynamic mode initialization. MS thesis, Naval Postgraduate School, Monterey, CA 93943, 68 pp.

Dewey, R.K., Moum, J.N., Paulson, C.A., Caldwell, D.R., Pierce, S.D., 1991. Structure and dynamics of a coastal filament. Journal of Geophysical Research 96, 14885–14908.

Dietrich, D.E., 1997. Application of a modified Arakawa "a" grid ocean model having reduced numerical dispersion to the Gulf of Mexico circulation. Dynamics of Atmospheres and Oceans 27, 201–217.

Dietrich, D.E., Ko, D.-S., 1994. A semi-collocated model based on the SOMS approach. International Journal of Numerical Methods in Fluids 99, 1103–1113.

Dietrich, D.E., Lin, C.A., 1994. Numerical studies of eddy shedding in the Gulf of Mexico. Journal of Geophysical Research 99, 7599–7615.

Eriksen, C.C., Weller, R.A., Rudnick, D.L., Pollard, R.T., Regier, L.A., 1991. Ocean frontal variability in the frontal air–sea interaction experiment. Journal of Geophysical Research 96, 8569–8591.

Gent, P.R., McWilliams, J.C., 1983. Consistent balanced models in bounded and periodic domains. Dynamics of Atmospheres and Oceans 7, 67–93.

Gill, A.E., 1982. Atmosphere-Ocean Dynamics. Academic Press, New York, NY, 662 pp.

Haney, R.L., Hale, R.A., Collins, C.A., 1995. Estimating subpycnocline density fluctuations in the California Current region from upper ocean observations. Journal of Atmospheric and Oceanic Technology 12, 550–566.

Holton, J.R., 1992. An Introduction to Dynamic Meteorology. 3rd edn. Academic Press, San Diego, CA, 511 pp.

Hoskins, B.J., Draghici, I., Davies, H.C., 1978. A new look at the $\tilde{\omega}$-equation. Quarterly Journal of the Royal Meteorological Society 104, 31–38.

Huang, X.-Y., Cederskov, A., Kallen, E., 1994. A comparison between digital filtering initialization and nonlinear normal-mode initialization in a data assimilation system. Monthly Weather Review 122, 1001–1015.

Huyer, A., Kosro, P.M., Fleischbein, J., Ramp, S.R., Stanton, T., Washburn, L., Chavez, F.P., Cowles, T.J., Pierce, S.D., Smith, R.L., 1991. Currents and water masses of the Coastal Transition Zone off Northern California, June to August 1988. Journal of Geophysical Research 96, 14809–14831.

Kadko, D.C., Washburn, L., Jones, B., 1991. Evidence of subduction within cold filaments of the Northern California Coastal Transition Zone. Journal of Geophysical Research 96, 14909–14926.

Leach, H., 1987. The diagnosis of synoptic-scale vertical motion in the seasonal thermocline. Deep-Sea Research 34, 2005–2017.

Lindstrom, S.S., Watts, D.R., 1994. Vertical motion in the Gulf Stream near 68°W. Journal of Physical Oceanography 24, 2321–2333.

Lorenz, E.N., 1992. The slow manifold—what is it? Journal of the Atmospheric Sciences 49, 2449–2451.

Lynch, P., Huang, X.-Y., 1992. Initialization of the HIRLAM model using a digital filter. Monthly Weather Review 120, 1019–1034.

Machenhauer, B., 1977. On the dynamics of gravity oscillations in a shallow water model with applications to normal model initialization. Beitraege zur Physik de Atmosphaere 50, 253–271.

Nuss, W.A., Titley, D.W., 1994. Use of multiquadric interpolation for meteorological objective analysis. Monthly Weather Review 122, 1611–1631.

Paduan, J.D., Niiler, P.P., 1990. A Lagrangian description of motion in northern California coastal transition filaments. Journal of Geophysical Research 95, 18095–18109.

Pedlosky, J., 1964. An initial value problem in the theory of baroclinic instability. Tellus 16, 12–17.

Pinot, J.-M., Tintore, J., Wang, D.-P., 1996. A study of the omega equation for diagnosing vertical motions at ocean fronts. Journal of Marine Research 54, 238–259.

Pollard, R.T., Regier, L., 1992. Vorticity and vertical circulation at an ocean front. Journal of Physical Oceanography 22, 609–625.

Ramp, S.R., Jensen, P.F., Brink, K.H., Niiler, P.P., Dagget, F.L., Best, J.S., 1991. The physical structure of cold filaments near Pt. Arena, California, during June 1987. Journal of Geophysical Research 96, 14859–14883.

Ramp, S.R., Rosenfeld, L.K., Tisch, T.D., Hicks, M.R., 1997. Moored observations of the current and temperature structure over the continental slope off central California: 1. A basic description of the variability. Journal of Geophysical Research 102, 22877–22902.

Rienecker, M.M., Mooers, C.N.K., Hagan, D.E., Robinson, A.R., 1985. A cool anomaly off Northern California: an investigation using IR imagery and in situ data. Journal of Geophysical Research 90, 4807–4818.

Rienecker, M.M., Mooers, C.N.K., Robinson, A.R., 1987. Dynamical interpolation and forecast of the evolution of mesoscale features off Northern California. Journal of Physical Oceanography 17, 1189–1213.

Rudnick, D.L., 1996. Intensive surveys of the Azores Front 2. Inferring the geostrophic and vertical velocity fields. Journal of Geophysical Research 101, 16291–16303.

Samelson, R.M., 1993. Linear instability of a mixed-layer front. Journal of Geophysical Research 98, 10195–10204.

Samelson, R.M., Chapman, D.C., 1995. Evolution of the instability of a mixed-layer front. Journal of Geophysical Research 100, 6743–6759.

Shearman, R.K., Barth, J.A., Allen, J.S., Haney, R.L., 2000. Diagnosis of the three dimensional circulation in mesoscale features with large Rossby number. Journal of Physical Oceanography 30, 2687–2709.

Strass, V.H., 1994. Mesoscale instability and upwelling: Part II. Testing the diagnostics of vertical motion with a three-dimensional ocean front model. Journal of Physical Oceanography 24, 1759–1767.

Strub, P.T., Kosro, P.M., Huyer, A., 1991. The nature of the cold filaments in the California Current system. Journal of Geophysical Research 96, 14743–14768.

Swenson, M.S., Niiler, P.P., Brink, K.H., Abbott, M.R., 1992. Drifter observations of a cold filament off Pt. Arena, California, in July 1988. Journal of Geophysical Research 97, 3593–3610.

Thomson, R.E., Papadakis, J.E., 1987. Upwelling filaments and motion of a satellite-tracked drifter along the west coast of North America. Journal of Geophysical Research 92, 6445–6461.

Tintore, J., Gomis, D., Alonso, S., Parrilla, G., 1991. Mesoscale dynamics and vertical motion in the Alboran Sea. Journal of Physical Oceanography 21, 811–823.

Viudez, A., Haney, R.L., Tintore, J., 1996. Circulation in the Alboran Sea as determined by quasi-synoptic hydrographic observations: Part II. Mesoscale ageostrophic motion diagnosed through density dynamical assimilation. Journal of Physical Oceanography 26, 706–724.

Walstad, L.J., Allen, J.S., Kosro, P.M., Huyer, A., 1991. Dynamics of the Coastal Transition Zone through data assimilation studies. Journal of Geophysical Research 96, 14959–14977.

Wang, D.P., 1993. Model of frontogenesis: subduction and upwelling. Journal of Marine Research 51, 497–513.

Washburn, L., Kadko, D.C., Jones, B.H., Hayward, T., Kosro, P.M., Stanton, T.P., Ramp, S., Cowles, T., 1991. Water mass subduction and the transport of phytoplankton in a coastal upwelling system. Journal of Geophysical Research 96, 14927–14946.